ResearchGate

See discussions, stats, and author profiles for this publication at: https://www.researchgate.net/publication/231150117

Overview of physical interaction models for photon and electron transport used in Monte Carlo codes

Article *in* Metrologia · March 2009

DOI: 10.1088/0026-1394/46/2/S08

CITATIONS
94

READS
4,194

2 authors:

Francesc Salvat
University of Barcelona
185 PUBLICATIONS **8,755** CITATIONS

SEE PROFILE

José M. Fernández-Varea
University of Barcelona
116 PUBLICATIONS **5,742** CITATIONS

SEE PROFILE

Some of the authors of this publication are also working on these related projects:

X-Ray Interactions View project

Electron bremsstrahlung cross sections: measurements in the São Paulo Microtron Accelerator View project

All content following this page was uploaded by Francesc Salvat on 02 June 2014.

The user has requested enhancement of the downloaded file.

IOPscience iopscience.iop.org

Home Search Collections Journals About Contact us My IOPscience

Overview of physical interaction models for photon and electron transport used in Monte Carlo codes

This article has been downloaded from IOPscience. Please scroll down to see the full text article.

2009 Metrologia 46 S112

(http://iopscience.iop.org/0026-1394/46/2/S08)

The Table of Contents and more related content is available

Download details:
IP Address: 129.78.139.28
The article was downloaded on 14/04/2010 at 07:16

Please note that terms and conditions apply.

IOP PUBLISHING METROLOGIA
Metrologia **46** (2009) S112–S138 doi:10.1088/0026-1394/46/2/S08

Overview of physical interaction models for photon and electron transport used in Monte Carlo codes

Francesc Salvat and José M Fernández-Varea

Facultat de Física (ECM and ICC), Universitat de Barcelona, Diagonal 647, ES-08028 Barcelona, Spain

E-mail: cesc@ecm.ub.es and jose@ecm.ub.es

Received 29 May 2008, in final form 12 September 2008
Published 20 March 2009
Online at stacks.iop.org/Met/46/S112

Abstract
The physical principles and approximations employed in Monte Carlo simulations of coupled electron–photon transport are reviewed. After a brief analysis of the assumptions underlying the trajectory picture used to generate random particle histories, we concentrate on the physics of the various interaction processes of photons and electrons. For each of these processes we describe the theoretical models and approximations that lead to the differential cross sections employed in general-purpose Monte Carlo codes. References to relevant publications and data resources are also provided.

1. Introduction

In the last few decades, with the availability of fast desktop computers and affordable memory storage, Monte Carlo simulation has become an essential tool in radiation physics. Because of the random nature of the interactions of radiation with matter, the evolution of electron–photon showers is a process particularly amenable to Monte Carlo simulation. Each interaction mechanism is characterized by a corresponding differential cross section (DCS), which determines the probability distribution of the various quantities relevant to that interaction (energy transfer, angular deflection of the projectile, energy and direction of generated secondary particles, if any, etc). Once the DCSs of the various interaction processes have been specified, Monte Carlo simulation reduces to routine numerical random sampling and particle tracking. However, even the most reliable DCSs available are obtained from *approximate* theoretical calculations and from experimental information and, consequently, they are affected by intrinsic uncertainties.

A number of Monte Carlo codes for the simulation of coupled electron–photon transport are available. Some of them (e.g. ETRAN (Berger and Seltzer 1988), ITS3 (Halbleib *et al* 1992), EGS4 (Nelson *et al* 1985), PENELOPE (Baró *et al* 1995, Salvat *et al* 2006), EGSnrc (Kawrakow and Rogers 2001), EGS5 (Hirayama *et al* 2006)) track only photons and electrons (and positrons). Other codes (most notably MCNP (X-5 Monte Carlo Team 2003), GEANT4 (Agostinelli *et al* 2003, Allison *et al* 2006) and FLUKA (Ferrari *et al* 2005)) allow tracking also neutrons and heavy charged particles.

In all existing codes, simulation of photon histories is performed by using a detailed (analogue) scheme, in which all interactions undergone by the transported photons are simulated in chronological succession. This strategy is applicable to radiations of any kind, whenever the number of interactions in each history is small or moderate. Indeed, a photon history terminates after a single photoelectric or pair-production interaction, or after a few Compton interactions (say, of the order of 10). With present-day computational facilities, detailed simulation of photon transport is a simple task.

Simulation of electron and positron transport is much more difficult than that of photon transport. The main reason is that the average energy loss of an electron in a single interaction is very small (of the order of a few tens of eV) and, therefore, high-energy electrons suffer a large number of collisions before being effectively slowed down to thermal energies. For high-energy electrons and positrons, most Monte Carlo codes have recourse to multiple-scattering theories which allow the simulation of the global effect of a large number of events in a track segment of a given length. Different schemes for condensed Monte Carlo simulation of high-energy charged particles are analysed in the seminal paper of Berger (1963). It should be noted that the multiple-scattering theories used in condensed simulations are only approximate (Berger and Wang 1988, Kawrakow and Bielajew 1998) and may lead

 © 2009 BIPM and IOP Publishing Ltd Printed in the UK

to systematic distortions of the results when the number of interactions undergone by the transported particles is small (plural scattering), as occurs, for example, in transmission through thin layers.

The aim of this paper is to describe the physical interaction models adopted in general-purpose Monte Carlo codes for the simulation of coupled electron–photon transport, and how the associated DCSs are derived or calculated. Emphasis is laid on the approximations underlying the theoretical models, and their limits of validity. Some of these approximations frequently pass unnoticed to the code users, not only because of the complexity of the theory, but also because code manuals usually provide only a superficial description of the interaction models employed. Although the list of references is not exhaustive, it includes the most relevant sources of numerical data used in Monte Carlo codes, as well as original publications and reviews on various aspects of radiation interactions that are of importance for transport simulation. A comparative analysis of sampling methods, multiple-scattering theories and electron/positron tracking algorithms (the so-called electron-transport mechanics) in the various codes is beyond the scope of this paper. The interested reader can find details in the user manuals of the codes, as well as in the publications cited above.

We limit our considerations to radiations with energies (kinetic energies in the case of electrons and positrons) in the range from about 1 keV up to ∼1 GeV. Simulations within this energy interval find applications in dosimetry, radiation shielding, medical diagnostic and radiotherapy, electron microscopy, x-ray fluorescence, detector design and characterization and other fields. At higher energies, physical processes not included in the theoretical formalism may take place with appreciable probabilities, e.g. in collisions of high-energy electrons with atoms, electron–positron pairs can be generated. At lower energies, interactions are affected by molecular binding and aggregation effects, which cannot be fully accounted for with the generic interaction models implemented in general-purpose codes. Special codes for the simulation of low-energy electron and positron transport in specific materials have been developed, mostly for applications in electron surface spectroscopies (Shimizu and Ding 1992, Jensen and Walker 1993, Fernández-Varea *et al* 1996) and microdosimetry (Nikjoo *et al* 2006).

The paper is organized as follows. Section 2 is devoted to fundamental approximations adopted in Monte Carlo transport simulation, including simplifications in the modelling of interactions and in the description of atomic structure. In section 3 we describe interaction models and data resources employed in general-purpose Monte Carlo codes to simulate photon interactions. Electron and positron collisions are considered in section 4. The relaxation of ions resulting from photon interactions or electron/positron impact is considered in section 5, which is followed by some concluding comments. The appendix contains a brief description of the Dirac equation and the relativistic distorted plane waves, which are used in most of the theoretical calculations that are referred to in the text.

2. General considerations

It is well known that the main advantages of Monte Carlo simulation are the ability to incorporate sophisticated interaction models and the ease of handling arbitrary geometries. The fact that these advantages stem from a number of drastic simplifications is not so common knowledge. Some of these simplifications set limits on the complexity of the physical interaction models that can be implemented in simulation codes and also on the energy range where simulation results are faithful. First of all, it is assumed that each material medium is homogeneous, isotropic and amorphous, with defined composition and density. The atoms or molecules in the medium are assumed to be randomly distributed with uniform density, i.e. in the case of solids, crystalline ordering is ignored. Moreover, molecular aggregation effects are disregarded, that is, molecules are considered as sets of individual atoms with *uncorrelated* positions. As a result, all material media are treated as if they were admixtures of *atomic* gases, with the same atomic concentrations as in the actual media. Energetic electrons or photons penetrating such a 'random scattering medium' are assumed to interact only with individual atoms, that is, the physics of the interactions is contained in the DCSs of atoms. In the case of compounds, this scheme is equivalent to using Bragg's additivity: the molecular cross section is set equal to the sum of the cross sections of the atoms that make up a molecule. Although molecular cross sections could in principle be used, at least for important specific materials (for instance water and air), such a sophistication is seldom implemented in high-energy codes. However, in the particular case of inelastic collisions of charged particles, molecular binding and aggregation effects are partially accounted for by using empirical values of the mean excitation energy of the considered materials, thus ensuring the correct high-energy collision stopping power (see section 4.2).

A basic assumption in both Monte Carlo simulation and elementary transport theory is that forces between beam particles are negligible. Consequently, these particles propagate independently of each other. In the Monte Carlo simulation, the transported (primary and secondary) particles follow straight trajectories between consecutive interactions. That is, wave-like characteristics are disregarded. This trajectory picture is justified only for high-energy radiation, whose wavelengths are much smaller than the average separation between the atoms in the material. When the wavelength is comparable to the interatomic distances, interference effects, resulting from the coherent superposition of waves scattered by different atoms, may become important and invalidate the trajectory picture. Thus, conventional Monte Carlo codes do not account for wave effects such as Bragg diffraction and channelling of charged particles in crystals.

In principle, individual interaction events should be simulated by random sampling from the associated DCSs. Very frequently, the DCS depends on several correlated variables (e.g. the energy loss and the scattering angle in the case of inelastic collisions of electrons) and, moreover, the DCSs may vary rapidly with the energy of the projectile.

Such DCSs are not practicable for Monte Carlo simulation, not only because of the large memory required to store the numerical DCSs (a three-dimensional table in the case of inelastic collisions) but also because random sampling from multivariate distributions is far more complicated, and slower, than from univariate distributions. A frequent practice is to disregard (or alter artificially) correlations between variables, normally by sampling the most relevant quantity from its marginal probability distribution and using approximate probability distributions for the other variables. The simulation of pair-production events (see section 3.4) provides a good example of this practical procedure. Approximations of this kind are employed in virtually all Monte Carlo codes and are expected to be harmless in the majority of applications, but they can cause visible distortions of the simulation results in cases where particles undergo a small number of interactions (e.g. in transmission through thin foils).

Owing to the wide energy range of interest, interactions must be treated using relativistic quantum mechanics. For electrons and positrons (mass m_e, charge $\pm e$) with kinetic energy E and momentum $\boldsymbol{p} = \hbar\boldsymbol{k}$ ($\hbar$ is the reduced Planck constant), we will frequently use the quantities

$$\gamma \equiv \frac{E + m_e c^2}{m_e c^2} = \sqrt{\frac{1}{1-\beta^2}} \qquad \text{and}$$

$$\beta = \frac{v}{c} = \sqrt{\frac{E(E+2m_e c^2)}{(E+m_e c^2)^2}} = \sqrt{\frac{\gamma^2-1}{\gamma^2}}, \tag{1}$$

which are, respectively, the total energy in units of the rest energy $m_e c^2$ and the velocity in units of the speed of light c. The wave number and wavelength of the electron are

$$k = (c\hbar)^{-1}\sqrt{E(E+2m_e c^2)} \qquad \text{and}$$

$$\lambda = \frac{2\pi}{k} = \frac{1.2398\,\text{nm}}{\sqrt{(E/\text{keV})[(E/\text{keV})+1022]}}, \tag{2}$$

respectively. The corresponding quantities for a photon of energy E are

$$k = (c\hbar)^{-1}E \qquad \text{and} \qquad \lambda = \frac{1.2398\,\text{nm}}{E/\text{keV}}. \tag{3}$$

2.1. Atomic structure

In the following we will consider interactions with neutral atoms of the element of atomic number Z. High-energy photons and charged particles interact with atoms primarily by producing excitations of the electron cloud. Although excitations of nuclei involve, on average, large energy transfers and may lead to nuclear activation, they have a small impact on the transport of photons and electrons and are often disregarded. Therefore, the nucleus can be considered as a passive distribution of electric charge. The finite size of the nucleus has a slight effect on the binding energies and wave functions of the inner shells of heavy atoms, and also on the DCS for elastic scattering of high-energy electrons. These effects can be accounted for by considering the distribution $\rho_{\text{nuc}}(r)$ of protons (or electric charge in units of e) in the nucleus, which is nearly spherically symmetric. The associated electrostatic potential is

$$\varphi_{\text{nuc}}(r) = e\int \frac{\rho_{\text{nuc}}(r')}{|\boldsymbol{r}-\boldsymbol{r}'|}\,\mathrm{d}\boldsymbol{r}' = \frac{4\pi e}{r}\int_0^r \rho_{\text{nuc}}(r')r'^2\,\mathrm{d}r' + 4\pi e\int_r^\infty \rho_{\text{nuc}}(r')r'\,\mathrm{d}r'. \tag{4}$$

For semi-quantitative calculations, we can describe the nucleus as a uniformly charged sphere of radius

$$R_{\text{nuc}} = 1.07\times 10^{-15}A^{1/3}\,\text{m}, \tag{5}$$

where A is the mass number. More realistic nuclear charge distributions are determined from electron-scattering experiments (Hofstadter 1956) or obtained from theoretical nuclear-structure models (see, for example, Richter and Brown 2003).

Because the mass of the target atom is much larger than the electron mass, in radiation transport theory and simulations the nucleus is normally regarded as having an infinite mass. This assumption implies that the nucleus can absorb any amount of recoil momentum without absorbing energy, a feature that simplifies the calculation of interaction cross sections.

When the energy of the radiation is higher than about 10 keV, interaction properties are not very sensitive to the fine details of atomic structure. As a consequence, it is sufficient to use relatively simple atomic models. In practice, simplifications in the description of atomic structure could be compensated *a posteriori* using empirical information. It should also be borne in mind that, although most theoretical calculations are based on free-atom models, material media are normally in condensed states. When aggregation effects are appreciable, they need to be modelled independently.

The state of the art in atomic-structure calculations is the self-consistent Dirac–Fock method (see, for example, Grant 1970, Desclaux 1975). The essential feature of the underlying physical picture is that electrons in different orbitals 'feel' different, non-local potentials. However, many calculations of interactions of high-energy radiation with atoms are based on simpler independent-particle approximations (IPA), in which atomic electrons are assumed to move independently in a common local central-field potential $V(r)$. The use of an IPA simplifies the calculation of atomic wave functions, ensures their orthogonality and, as a consequence, facilitates the evaluation of transition matrix elements, which satisfy strong selection rules (e.g., only single-electron transitions are allowed when interactions of atoms with radiation are treated as first-order perturbations). Without these simplifications, most calculations would be virtually impossible.

In the IPA, atomic wave functions are represented by single Slater determinants,

$$\Psi \equiv \frac{1}{\sqrt{Z!}}\begin{vmatrix} \psi_1(\boldsymbol{r}_1) & \dots & \psi_1(\boldsymbol{r}_Z) \\ \vdots & \ddots & \vdots \\ \psi_Z(\boldsymbol{r}_1) & \dots & \psi_Z(\boldsymbol{r}_Z) \end{vmatrix}, \tag{6}$$

where the one-electron orbitals $\psi_i(\boldsymbol{r})$ are solutions of the Dirac equation

$$[c\widetilde{\boldsymbol{\alpha}}\cdot\boldsymbol{p} + (\widetilde{\beta}-1)m_e c^2 + V(r)]\psi_i(\boldsymbol{r}) = E_i\psi_i(\boldsymbol{r}). \tag{7}$$

The (bound) orbitals $\psi_i(\boldsymbol{r})$ are of the form given by equation (A.4), that is, they are identified by the quantum numbers n, ℓ and j (or κ) and m. The energy of each atomic state Ψ is determined by the electronic configuration, that is, by the set of single-electron levels $n\ell j$ that are occupied and the corresponding occupancy numbers q ($\leqslant 2j+1$). A configuration

$$(n_1\ell_1 j_1)^{q_1}, \quad (n_2\ell_2 j_2)^{q_2}, \ldots \tag{8}$$

consists of shells $n_1\ell_1 j_1$, $n_2\ell_2 j_2$, ... with q_1, q_2, ... electrons, respectively. The electron density corresponding to the state Ψ is

$$\rho(r) \equiv \sum_{i=1}^{Z} |\psi_i(\boldsymbol{r})|^2 = \frac{1}{4\pi r^2} \sum_a q_a [P^2_{n_a\kappa_a}(r) + Q^2_{n_a\kappa_a}(r)], \tag{9}$$

where the last summation runs over the occupied shells, and $P_{n_a\kappa_a}(r)$ and $Q_{n_a\kappa_a}(r)$ are the radial wave functions of the orbitals in shell $n_a\ell_a j_a$. In the case of closed-shell configurations (with $q_a = 2j_a + 1$), the electron density and the electrostatic potential are spherically symmetric and, consequently, the central-field approximation is expected to be fairly accurate. Note that for open shells (with $q_a < 2j_a + 1$) the electron density, which is not spherical, is replaced by a spherical average. The electrostatic potential of the electron cloud is

$$\varphi_{\rm el}(r) = -e \int \frac{\rho(r')}{|\boldsymbol{r} - \boldsymbol{r}'|}\, {\rm d}\boldsymbol{r}' = -\frac{4\pi e}{r} \int_0^r \rho(r') r'^2\, {\rm d}r' - 4\pi e \int_r^\infty \rho(r') r'\, {\rm d}r'. \tag{10}$$

Many calculations of radiation interactions utilize the Dirac–Hartree–Fock–Slater (DHFS) self-consistent potential. This potential is given by

$$V_{\rm DHFS}(r) = V_{\rm nuc}(r) + V_{\rm el}(r) + V_{\rm ex}(r), \tag{11}$$

where $V_{\rm nuc}(r) = -e\varphi_{\rm nuc}(r)$ and $V_{\rm el}(r) = -e\varphi_{\rm el}(r)$ are the electrostatic interaction energies of the electron with the nucleus and the electron cloud, respectively, and

$$V_{\rm ex}(r) = -e^2 \frac{3}{2} \left(\frac{3}{\pi}\rho(r)\right)^{1/3} \tag{12}$$

is Slater's (1951) local approximation to the exchange potential, which results from assuming that the exchange charge distribution is the same as if the electron were immersed in a homogeneous electron gas with density equal to the local electron density $\rho(r)$. This simplification is not accurate at large radii, where $\rho(r)$ is very small, and the potential given by equation (11) incorrectly vanishes at large distances. To get a potential with the correct asymptotic behaviour ($= -e^2/r$) it is customary to introduce an ad hoc correction, known as the Latter tail (Latter 1955), which consists of replacing $V_{\rm DHFS}(r)$ by $-e^2/r$ at large radii, where expression (11) gives values larger than $-e^2/r$. The DHFS potential is calculated self-consistently, usually for the ground-state configuration of the atom. A computer program that calculates DHFS orbitals, energy eigenvalues and electronic densities has been written by Liberman *et al* (1971).

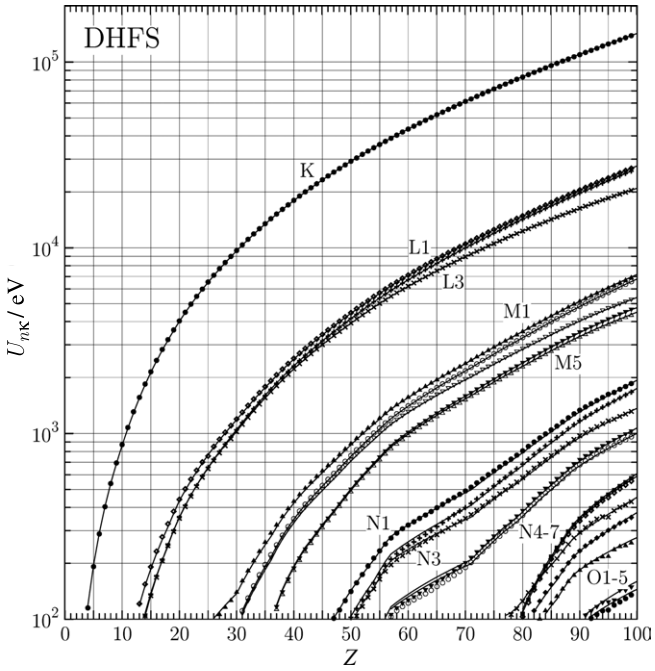

Figure 1. Shell ionization energies of neutral atoms, $U_{n\kappa}$, in electron volts. Symbols represent the ionization energies recommended by Carlson (1975), from a combination of experimental data and theoretical calculations. Lines indicate the one-electron energy levels of the DHFS potential, with reversed sign, $-E_{n\kappa}$.

It is worth mentioning that the DHFS model implies a number of approximations. First, the non-local exchange interaction in the Dirac–Fock equations is approximated by Slater's local potential. Moreover, the use of a single Slater determinant as the atomic wave function amounts to neglecting electron correlations other than those implied by the antisymmetry of the wave function. Nevertheless, DHFS electron densities do not differ appreciably from Dirac–Fock densities. A peculiarity of the DHFS model, with Latter's tail correction, is that experimental ionization energies $U_{n\kappa}$ of inner shells are very close to the negative eigenvalues of equation (7), $U_{n\kappa} \approx -E_{n\kappa}$ (see figure 1). These features make the DHFS model well suited for high-energy radiation interaction calculations.

3. Photon interactions

In the considered energy range, the dominant interactions of photons with atoms are photoelectric absorption, Rayleigh (coherent) scattering, Compton (incoherent) scattering and electron–positron pair production (Hubbell 1999). Photonuclear absorption occurs with appreciable probability only for photons with energies between ~5 MeV and 50 MeV (see, for example, Hubbell *et al* 1980, and references therein); the corresponding total cross section has a broad peak (the so-called giant resonance) with a maximum value smaller than the total cross section for 'electronic interactions' by a factor of the order of 10. As indicated above, photonuclear absorption

has a small effect on transport calculations and it may be disregarded in the majority of practical applications.

In each interaction, the primary photon is absorbed. In the case of scattering, coherent or incoherent, a secondary photon is re-emitted. Although the net effect of a scattering event is analogous to a change in the direction and energy of the photon, this change occurs through absorption and re-emission of quanta. This behaviour is at variance with that of charged particles, which may lose only part of their energy in each interaction (see section 4). The most accurate description of photon interactions is obtained within the framework of quantum electrodynamics. Nevertheless, for radiations with energies of less than about 20 keV, conventional perturbation theory and non-relativistic quantum mechanics (see, for example, Baym 1974) also yield realistic results.

Electromagnetic radiation is treated by using the formalism of second quantification. Since calculations are performed in a reference frame where the atom (and the material medium) is at rest, it is convenient to use the Coulomb gauge. In this gauge, and in the Gaussian system of units, the electromagnetic field in vacuum is represented by the vector potential operator (Baym 1974, Sakurai 1967)

$$\boldsymbol{A}(\boldsymbol{r},t)=\sum_{\boldsymbol{k},\alpha}\sqrt{\frac{2\pi\hbar c^2}{\omega}}\{a_{\boldsymbol{k}\alpha}\hat{\boldsymbol{\epsilon}}_\alpha\exp[\mathrm{i}(\boldsymbol{k}\cdot\boldsymbol{r}-\omega t)] + a^\dagger_{\boldsymbol{k}\alpha}\hat{\boldsymbol{\epsilon}}^*_\alpha\exp[-\mathrm{i}(\boldsymbol{k}\cdot\boldsymbol{r}-\omega t)]\}, \tag{13}$$

where $a^\dagger_{\boldsymbol{k}\alpha}$ and $a_{\boldsymbol{k}\alpha}$ are creation and annihilation operators, respectively, and the sum is over wave vectors $\boldsymbol{k}$ and over two orthogonal linear polarization states $\hat{\boldsymbol{\epsilon}}_\alpha$ ($\alpha = 1, 2$). The angular frequency ω, wave number k and energy E of each mode $\boldsymbol{k}\alpha$ are related through $E = \hbar\omega = c\hbar k$. The constant under the square root in equation (13) corresponds to monochromatic plane waves obeying periodic boundary conditions on a cubic box with edges of unit length.

As mentioned above, atomic states are usually described by means of an IPA, that is, as single Slater determinants, equation (6). Cross sections are calculated by treating the interaction between the electromagnetic field and the target atom as a perturbation, to lowest non-vanishing perturbation order. Generally, when the final state contains free particles (photons or electrons), the transition rate is calculated using Fermi's golden rule (see, for example, Sakurai 1967), and the DCS is obtained as the ratio of that transition rate to the fluence rate of incident photons. The calculation involves matrix elements of the (dimensionless) operator

$$M_{\boldsymbol{k}\alpha}\equiv\hat{\boldsymbol{\epsilon}}_\alpha\cdot\sum_{i=1}^{Z}\widetilde{\boldsymbol{\alpha}}_i\exp(\mathrm{i}\boldsymbol{k}\cdot\boldsymbol{r}_i), \tag{14}$$

where the summation is over the Z atomic electrons. This operator describes absorption of a $\boldsymbol{k}\alpha$ photon by the atom; its Hermitian conjugate $M^\dagger_{\boldsymbol{k}\alpha}$ describes the emission of a photon. Since these are symmetric one-body operators, their matrix elements between Slater determinants, $\langle\Psi_B|M_{\boldsymbol{k}\alpha}|\Psi_A\rangle$, can be reduced to a sum of matrix elements of a one-electron operator. This is accomplished by straight application of the Slater–Condon rules (Condon 1930). When Ψ_A and Ψ_B differ in more than one orbital, these rules imply that $\langle\Psi_B|M_{\boldsymbol{k}\alpha}|\Psi_A\rangle = 0$ (as a consequence of the orthogonality of one-electron orbitals). Therefore, the only possible transitions are between states whose Slater determinants differ in just one orbital, i.e. single-electron transitions. Let ψ_a and ψ_b denote the differing orbitals in Ψ_A and Ψ_B, respectively. We have

$$\begin{aligned}\langle\Psi_B|M_{\boldsymbol{k}\alpha}|\Psi_A\rangle &= \left\langle\Psi_B\left|\hat{\boldsymbol{\epsilon}}_\alpha\cdot\sum_{i=1}^{Z}\widetilde{\boldsymbol{\alpha}}_i\exp(\mathrm{i}\boldsymbol{k}\cdot\boldsymbol{r}_i)\right|\Psi_A\right\rangle\\ &= \langle\psi_b|\hat{\boldsymbol{\epsilon}}_\alpha\cdot\widetilde{\boldsymbol{\alpha}}\exp(\mathrm{i}\boldsymbol{k}\cdot\boldsymbol{r})|\psi_a\rangle\\ &\equiv (M_{\boldsymbol{k}\alpha})_{ba}.\end{aligned} \tag{15}$$

We are thus led to the so-called *one-active-electron approximation*, which consists of considering only the excitations of a single electron from a bound orbital ψ_a to an unoccupied (bound or free) orbital ψ_b, whereas the other atomic electrons behave as mere spectators and their orbitals remain frozen in the course of the interaction.

Elementary quantum electrodynamics deals with free electrons and positrons described in the second-quantification formalism, with states of these particles represented as Dirac plane waves. More elaborate quantum electrodynamics calculations of interactions with atoms are performed using the so-called Furry picture, in which the interaction of the electrons with the atomic field, represented by a certain potential $V(r)$, is incorporated in the unperturbed Hamiltonian. That is, electron wave functions are solutions of the one-electron Dirac equation (7), which can be solved numerically to very high accuracy, and only a fraction of the interaction needs to be treated (approximately) as a perturbation. With a weaker interaction, calculations in the lowest non-vanishing order of perturbation theory should yield more accurate results. In the theoretical interaction models presented below, the states of free electrons or positrons are distorted plane waves, that is, exact solutions of the Dirac equation for the potential $V(r)$ which, at large radial distances, behave as a plane wave plus a spherical (incoming or outgoing) wave (see the appendix).

3.1. Photoelectric effect

In the photoelectric effect, a photon in the mode $\boldsymbol{k}\alpha$, with energy E, is absorbed and an electron makes a transition from a bound orbital ψ_a of energy E_a to a final free orbital with kinetic energy $E_b = E_a + E$ and momentum $\hbar\boldsymbol{k}_b$. The elementary theory of the atomic photoeffect has been reviewed by Pratt *et al* (1973). The interaction between the active electron and the electromagnetic field is treated in first-order perturbation theory, and the wave function of the ejected photoelectron is represented as a distorted plane wave with *incoming* spherical distortion, $\psi_b = \psi^{(-)}_{\boldsymbol{k}_b m_{\mathrm{S}b}}$, equation (A.18).

The partial photoelectric cross section of a closed electron shell $n_a\ell_a j_a$ is obtained by summing the contributions of the $2j_a + 1$ orbitals of that shell. It is usually assumed that the incident photon beam is unpolarized, and that the spin of the photoelectron is not observed. With these assumptions, the partial DCS for photoionization of the active shell is a function of only the direction $\hat{\boldsymbol{k}}_b$ of the photoelectron. It is given by

$$\frac{\mathrm{d}\sigma_{\mathrm{ph},a}}{\mathrm{d}\hat{\boldsymbol{k}}_b}=(2\pi)^2e^2\hbar c\frac{1}{E}k_b\frac{E_b+m_\mathrm{e}c^2}{c^2\hbar^2}\sum{}'|(M_{\boldsymbol{k}\alpha})_{ba}|^2, \tag{16}$$

where the primed summation sign denotes a sum over the orbitals in the shell and over the spin states of the emerging electron, as well as an average over polarization directions of the incident photon. The global factor in this equation depends on the adopted normalization for free-state electron wave functions, which determines the 'number of states per unit final energy' that occurs in Fermi's golden rule. Here, and in the following sections, we assume the normalization given by equation (A.15). The numerical calculation of the DCS is performed by making a multipole expansion of the radiation field and using the partial-wave expansion in equation (A.13) of the distorted plane wave of the electron (Scofield 1989).

The shell cross section, $\sigma_{\mathrm{ph},a}$, is obtained by integrating the DCS given by equation (16) over photoelectron directions (and averaging over occupied orbitals in the case of open shells). This integration (and average) simplifies the whole calculation, since angular integrals are evaluated analytically and only radial integrals have to be calculated numerically (Pratt *et al* 1973). The total atomic cross section is the sum of contributions of the various shells of the ground-state configuration. Calculations of the photoeffect for electrons in a pure Coulomb field (i.e. using the potential $V(r) = -Ze^2/r$) were reported by Pratt *et al* (1964) and by Alling and Johnson (1965). Calculations for screened Coulomb fields, typically the DHFS field, are described by Pratt *et al* (1973) and by Scofield (1989).

Since the DCS given by equation (16) cannot be expressed in analytical form, a common practice in Monte Carlo simulations is to sample the direction of the emitted photoelectron from the approximate DCS obtained by Sauter (1931). This DCS describes the ionization of the ground state ($1s_{1/2}$) of hydrogenic ions, and is obtained in the plane-wave Born approximation (i.e. with the final state of the photoelectron ψ_b represented by a plane wave). The Sauter DCS (per electron) is given by

$$\frac{\mathrm{d}\sigma_{\mathrm{ph}}}{\mathrm{d}\hat{\boldsymbol{k}}_b} = \alpha^4 r_{\mathrm{e}}^2 \left(\frac{Zm_{\mathrm{e}}c^2}{E}\right)^5 \frac{\beta^3}{\gamma} \frac{\sin^2\theta_{\mathrm{e}}}{(1-\beta\cos\theta_{\mathrm{e}})^4} \times \left[1 + \frac{1}{2}\gamma(\gamma-1)(\gamma-2)(1-\beta\cos\theta_{\mathrm{e}})\right], \qquad (17)$$

where θ_{e} is the angle between the directions of the photoelectron and the incident photon, $\alpha = e^2/(\hbar c)$ is the fine-structure constant, $r_{\mathrm{e}} = e^2/(m_{\mathrm{e}}c^2)$ is the classical electron radius and the quantities γ and β are the reduced energy and velocity of the emitted photoelectron, equations (1). It should be noted that this DCS is obtained by neglecting the distortion that the atomic field causes on the wave function of the emerging electron. The difference between the Sauter *angular distribution* and the exact distribution (for a pure Coulomb field) has been analysed by Pratt *et al* (1964). These authors found that the distributions agree closely for atomic numbers up to ~50, but the differences become significant for higher atomic numbers (~25% for $Z = 84$ and $E = 662$ keV) and decrease when the photon energy increases.

In principle, Sauter's angular distribution applies only to the ionisation of the K shell of not too heavy atoms by high-energy photons. Nevertheless, in many practical simulations no appreciable errors are introduced when Sauter's distribution is used to describe any photoionization event, irrespective of the atomic shell and the photon energy. The main reason is that the emitted photoelectron immediately starts to interact with the medium, and its direction of movement is strongly altered after travelling a path length much shorter than the photon mean free path. On the other hand, when the photon energy exceeds the K edge, most of the ionizations occur in the K shell and then the Sauter distribution represents a fairly good approximation.

The most extensive tables of atomic photoelectric cross sections available are those of the Evaluated Photon Data Library (EPDL97) of Cullen *et al* (1997), which includes partial shell cross sections and total atomic cross sections for all the elements from hydrogen ($Z = 1$) to lawrencium ($Z = 100$) and photon energies E from 10 eV to 100 GeV. For energies from the absorption edge to 1 MeV, the tabulated cross sections were computed according to equation (16) using Scofield's computer program. For energies higher than 1 MeV, calculated shell cross sections were scaled to match the total cross sections of Hubbell *et al* (1980). Note that shell cross sections are needed for sampling the active shell in each photoabsorption event. The XCOM program (Berger *et al* 2005) also provides total atomic cross sections for photon energies between 1 keV and 100 GeV, which are essentially the same as in the EPDL97 library. Henke *et al* (1993) have published tables of total atomic cross sections for the elements $Z = 1$ to 92, and for a more limited range of photon energies extending from 50 eV to 30 keV, which were generated from a compilation of experimental data and theoretical calculations.

It should be mentioned that these cross sections pertain to free atoms. Cross sections for photoabsorption by atoms bound in molecules and solids are different, because neighbour atoms alter the wave function of the emerging photoelectron. The main effect of aggregation is an oscillatory structure in the photoabsorption cross section, for energies just above an absorption edge, known as x-ray absorption fine structure. The theory of this effect is reviewed by Rehr and Albers (2000).

3.2. Rayleigh scattering

Here, and in the next section, we consider photon scattering processes, that is, interactions in which an incident photon in the mode $\boldsymbol{k}\alpha$ is absorbed by the target atom and a photon $\boldsymbol{k}'\alpha'$ is emitted, while the active atomic electron makes a transition from its initial orbital ψ_a to a final orbital ψ_b. Since the process involves two photons, it is described using second-order perturbation theory. The transition rate is determined by the transition matrix element (Akhiezer and Berestetskii 1965, Baym 1974)

$$\mathcal{T}_{b,\boldsymbol{k}'\alpha';a,\boldsymbol{k}\alpha} \equiv -m_{\mathrm{e}}c^2 \sum_n \left[\frac{(M^{\dagger}_{\boldsymbol{k}'\alpha'})_{bn}(M_{\boldsymbol{k}\alpha})_{na}}{\mathcal{W}_n - \mathcal{W}_a - E - \mathrm{i}\eta} + \frac{(M_{\boldsymbol{k}\alpha})_{bn}(M^{\dagger}_{\boldsymbol{k}'\alpha'})_{na}}{\mathcal{W}_n - \mathcal{W}_a + E' - \mathrm{i}\eta}\right] \qquad (18)$$

and by energy conservation,

$$E' = E + \mathcal{W}_a - \mathcal{W}_b. \qquad (19)$$

The quantity $\mathcal{W}_n = E_n + m_e c^2$ is the total energy (including the rest energy) of the electron in the orbital ψ_n. The summation is over all, positive- and negative-energy intermediate one-electron states ψ_n. This calculation scheme is frequently referred to as the second-order S-matrix method.

Rayleigh scattering, also called coherent scattering, is the elastic scattering of photons, without electronic excitation of the target atom ($E' = E$, $\psi_b = \psi_a$). The DCS for Rayleigh scattering of polarized photons by a free atom is given by

$$\frac{\mathrm{d}\sigma_{\mathrm{Ra}}}{\mathrm{d}\hat{\boldsymbol{k}}'} = r_e^2 {\sum_{a}}' |\mathcal{T}_{a,\boldsymbol{k}'\alpha';a,\boldsymbol{k}\alpha}|^2, \tag{20}$$

where the primed summation is over the filled orbitals ψ_a of the ground-state configuration (with the usual average in the case of open shells), and over possible degenerate final states ψ_b of the active electron, excluding orbitals that are occupied by other atomic electrons. A detailed description of the calculation of cross sections for Rayleigh scattering is given by Cromer and Liberman (1970). To express the DCS in a form that resembles the non-relativistic result (as given, for example, by Sakurai 1967), they set

$$\mathcal{T}_{a,\boldsymbol{k}'\alpha';a,\boldsymbol{k}\alpha} = -(\hat{\boldsymbol{\epsilon}}^*_{\alpha'} \cdot \hat{\boldsymbol{\epsilon}}_{\alpha}) \langle \psi_a | \exp[\mathrm{i}(\boldsymbol{k} - \boldsymbol{k}') \cdot \boldsymbol{r}] | \psi_a \rangle + f'_a + \mathrm{i} f''_a. \tag{21}$$

The first term on the right-hand side is proportional to the form factor of the active orbital,

$$F_a(\boldsymbol{q}) \equiv \langle \psi_a | \exp(\mathrm{i}\boldsymbol{q} \cdot \boldsymbol{r}) | \psi_a \rangle = \int |\psi_a(\boldsymbol{r})|^2 \exp(\mathrm{i}\boldsymbol{q} \cdot \boldsymbol{r})\, \mathrm{d}\boldsymbol{r}, \tag{22}$$

where $\hbar\boldsymbol{q} = \hbar\boldsymbol{k} - \hbar\boldsymbol{k}'$ is the momentum transfer to the atom. Note that, for elastic scattering, $k' = k$ and

$$q = 2k \sin(\theta/2). \tag{23}$$

The quantity $f'_a + \mathrm{i} f''_a$ is known as the anomalous scattering factor or as the dispersion correction to the form factor. The adjective 'anomalous' refers to the fast variation of this quantity for photon energies around the absorption edge.

For unpolarized incident photons, and when the polarization of the scattered photons is not observed, the atomic DCS for Rayleigh scattering is given by

$$\frac{\mathrm{d}\sigma_{\mathrm{Ra}}}{\mathrm{d}\hat{\boldsymbol{k}}'} = r_e^2 \frac{1 + \cos^2\theta}{2} |F(q, Z) + f' + \mathrm{i} f''|^2, \tag{24}$$

where

$$F(q, Z) = \sum_a F_a(\boldsymbol{q}) = \int \rho(r) \exp(\mathrm{i}\boldsymbol{q} \cdot \boldsymbol{r}) \mathrm{d}\boldsymbol{r} \tag{25}$$

is the atomic form factor, i.e. the Fourier transform of the electron density. For a spherical electron density, the integral over directions can be performed analytically, and we have

$$F(q, Z) = \frac{4\pi}{q} \int_0^\infty \rho(r) \sin(qr) r \, \mathrm{d}r. \tag{26}$$

Hubbell *et al* (1975, 1977) have published tables of atomic form factors, mostly obtained from non-relativistic Hartree–Fock electron densities. The EPDL97 library (Cullen *et al* 1997) contains a more detailed tabulation of Hubbell's form factors.

Numerical S-matrix calculations indicate that, for energies below the absorption edge of the K shell, the anomalous scattering factors are practically independent of the scattering angle θ (see, for example, Kissel *et al* 1995, and references therein). Hence, $f' + \mathrm{i} f''$ can be approximated by its value at $\theta = 0$, which can be obtained from dispersion relations that follow from the analytic nature of the scattering amplitude and from causality requirements. Similar considerations in classical dielectric theory lead to essentially equivalent results (see, for example, James 1948, Henke *et al* 1993). The angle-independent anomalous scattering factor is given by

$$f'(E) = -(Z/82.5)^{2.37} + \frac{1}{\pi^2 r_e \hbar c} \mathsf{P} \int_0^\infty \frac{W^2 \sigma_{\mathrm{ph}}(W)}{E^2 - W^2} \, \mathrm{d}W \tag{27}$$

and

$$f''(E) = \frac{1}{4\pi r_e \hbar c} E \sigma_{\mathrm{ph}}(E), \tag{28}$$

where $\sigma_{\mathrm{ph}}(E)$ is the atomic photoelectric cross section for photons of energy E and P indicates the principal value of the integral.

The tables of Henke *et al* (1993) include anomalous scattering factors for the elements $Z = 1$ to 92 and photon energies between 50 eV and 30 keV. An extensive tabulation of anomalous scattering factors, covering all the elements up to $Z = 100$ and energies between 1 eV and 10 MeV has been prepared by Cullen (1989).

3.3. Compton scattering

In Compton scattering, the incident photon $\boldsymbol{k}\alpha$ is absorbed and a scattered photon $\boldsymbol{k}'\alpha'$ of lower energy is emitted. The energy difference between the incident and scattered photons is transferred to an atomic electron in the orbital $\psi_a(\boldsymbol{r})$ that makes a transition to a positive-energy free orbital $\psi_b(\boldsymbol{r})$, which is represented by a distorted plane wave $\psi^{(-)}_{\boldsymbol{k}_b m_{Sb}}(\boldsymbol{r})$ with momentum $\hbar\boldsymbol{k}_b$ and spin m_{Sb}. Since the mass of the target atom is much larger than the electron mass, the atom can absorb any amount of recoil momentum and, consequently, the directions of the scattered photon and the electron are not constrained by kinematics.

Assuming that the spin of the ejected electron is not observed, the DCS for scattering by electrons of a closed shell $n_a \ell_a j_a$ is given by

$$\frac{\mathrm{d}^3\sigma_{\mathrm{Co},a}}{\mathrm{d}E' \mathrm{d}\hat{\boldsymbol{k}}' \mathrm{d}\hat{\boldsymbol{k}}_b} = r_e^2 \frac{E'}{E} k_b \frac{E_b + m_e c^2}{c^2 \hbar^2} {\sum_{b,\boldsymbol{k}'\alpha';a,\boldsymbol{k}\alpha}}' |\mathcal{T}_{b,\boldsymbol{k}'\alpha';a,\boldsymbol{k}\alpha}|^2, \tag{29}$$

where E and E' are the energies of the incident and scattered photons, respectively, and the summation is over the orbitals of the active shell. The numerical factor before the sum arises from the density of continuum electron states. Calculations of Compton scattering following this second-order S-matrix method have been reported by Bergstrom *et al* (1993). These calculations are very complicated, and the results cannot be reduced to a compact form suited for simulation purposes.

A limiting situation that can be described analytically is that of Compton scattering by free electrons at rest, which was first studied by Klein and Nishina in 1929. In this case, the initial and final states of the target electron can be represented as discrete plane waves satisfying periodic boundary conditions on a cubic box of unit volume. The calculation involves the use of energy-projection tricks; a detailed description of the formal technique can be found, for example, in Heitler's (1984) book. The final result is the Klein–Nishina DCS,

$$\frac{\mathrm{d}\sigma^{(\mathrm{KN})}}{\mathrm{d}\hat{\boldsymbol{k}}'} = r_\mathrm{e}^2 \frac{1}{4}\frac{E'^2}{E^2}\left[\frac{E}{E'}+\frac{E'}{E}-2+4(\hat{\boldsymbol{\epsilon}}_{\alpha'}\cdot\hat{\boldsymbol{\epsilon}}_{\alpha})^2\right], \tag{30}$$

which describes the scattering of linearly polarized photons by free electrons at rest. Because of energy-momentum conservation, the energy E' of the scattered photon depends only on the scattering angle θ, and is given by

$$E' = \frac{E}{1+(E/m_\mathrm{e}c^2)(1-\cos\theta)} \equiv E_\mathrm{C}. \tag{31}$$

The DCS for the scattering of unpolarized photons is obtained by summing and averaging over, respectively, final and initial polarization states (see, for example, Sakurai (1967), pp 51 and 52). The result is

$$\frac{\mathrm{d}\sigma^{(\mathrm{KN})}}{\mathrm{d}\hat{\boldsymbol{k}}'} = r_\mathrm{e}^2 \frac{1}{2}\frac{E'^2}{E^2}\left(\frac{E}{E'}+\frac{E'}{E}-\sin^2\theta\right). \tag{32}$$

The Klein–Nishina DCS provides a reliable description of Compton scattering by atoms only for those interactions where the momentum transfer $\hbar q$ ($\hbar\boldsymbol{q} = \hbar\boldsymbol{k} - \hbar\boldsymbol{k}'$) is much larger than the average momentum of the active electron. A more realistic description is provided by the impulse approximation (Ribberfors 1975), which assumes that the electrons in the active shell $n_a\ell_a j_a$ react essentially as if they were free electrons moving with a momentum distribution $\rho_a(\boldsymbol{p})$, which is spherically symmetrical for closed shells. That is, the DCS for Compton scattering by the active shell is given by

$$\mathrm{d}\sigma^{(\mathrm{IA})}_{\mathrm{Co},a} = \Theta(W - U_{n_a\kappa_a})\int \mathrm{d}\boldsymbol{p}\rho_a(\boldsymbol{p})\,\mathrm{d}\sigma^{(\mathrm{free})}(\boldsymbol{p}), \tag{33}$$

where $\mathrm{d}\sigma^{(\mathrm{free})}(\boldsymbol{p})$ denotes the DCS for collisions of the projectile with a *free* electron that moves with momentum $\boldsymbol{p}$ and W is the energy transferred in the interaction, $W = E - E'$. The unit step function $\Theta(x)$ (= 1 if $x > 0$, and = 0 otherwise) accounts for the fact that only energy transfers W larger than the ionization energy $U_{n_a\kappa_a}$ of the active shell can produce ionizations. The momentum distribution $\rho_a(\boldsymbol{p})$ of the electrons in the active shell can be obtained from the Fourier transforms of the orbitals $\psi_a(\boldsymbol{r})$ (see, for example, Segui *et al* 2002).

To allow the evaluation of the integral in equation (33), Ribberfors used the Klein–Nishina DCS expressed in covariant form (so that its dependence on the initial momentum of the target electron is explicit) and, after certain simplifications, obtained the following expression for the Compton DCS (Ribberfors and Berggren 1982, see also Brusa *et al* 1996),

$$\frac{\mathrm{d}^2\sigma^{(\mathrm{IA})}_{\mathrm{Co},a}}{\mathrm{d}E'\,\mathrm{d}\hat{\boldsymbol{k}}'} = \frac{r_\mathrm{e}^2}{2}\frac{E'm_\mathrm{e}c}{Ec\hbar q}\left[1+\left(\frac{p_z}{m_\mathrm{e}c}\right)^2\right]^{-1/2} X J_a(p_z), \tag{34}$$

where

$$c\hbar q = \sqrt{E^2 + E'^2 - 2EE'\cos\theta}. \tag{35}$$

The quantity p_z is the projection of the initial momentum $\boldsymbol{p}$ of the active electron on the direction of the vector $-\boldsymbol{q}$, and it is given by

$$p_z \equiv -\frac{\boldsymbol{p}\cdot\boldsymbol{q}}{q} \simeq \frac{EE'(1-\cos\theta) - m_\mathrm{e}c^2(E-E')}{c^2\hbar q} \tag{36}$$

or, equivalently,

$$\frac{p_z}{m_\mathrm{e}c} = \frac{E(E'-E_\mathrm{C})}{E_\mathrm{C}c\hbar q}, \tag{37}$$

where E_C is the energy of the Compton line (given by expression (31)), i.e. the energy of photons scattered in the direction θ by *free electrons at rest* ($p = 0$).

The function X in equation (34) is

$$X \equiv \frac{R}{R'} + \frac{R'}{R} + 2\left(\frac{1}{R}-\frac{1}{R'}\right) + \left(\frac{1}{R}-\frac{1}{R'}\right)^2 \tag{38}$$

with

$$R = \frac{E}{m_\mathrm{e}c^2}\left\{\left[1+\left(\frac{p_z}{m_\mathrm{e}c}\right)^2\right]^{1/2} + \frac{E - E'\cos\theta}{c\hbar q}\frac{p_z}{m_\mathrm{e}c}\right\} \tag{39}$$

and

$$R' = R - \frac{E'}{m_\mathrm{e}c^2}\left(\frac{E}{E_\mathrm{C}}-1\right), \tag{40}$$

and $J_a(p_z)$ is the Compton profile of the active electron shell,

$$J_a(p_z) \equiv \iint \rho_a(\boldsymbol{p})\,\mathrm{d}p_x\,\mathrm{d}p_y = 2\pi\int_{|p_z|}^{\infty}\rho_a(p)p\,\mathrm{d}p, \tag{41}$$

where the last equality follows from the spherical symmetry of the electron density $\rho_a(p)$ of the shell. Extensive tables of Hartree–Fock Compton profiles for the elements have been published by Biggs *et al* (1975).

The motion of the atomic electrons causes the so-called Doppler broadening of the energy distribution of the scattered photons. Photons that are scattered in directions forming an angle θ with the direction of incidence have a continuous energy distribution, with a maximum at the Compton energy, given by equation (31). This results from the fact that the frequency of the incident photon is Doppler shifted when observed from a Lorentz frame moving with the same velocity as the target electron. The main effect of binding is to prevent transitions that would lead the active electron to final bound orbitals. Note that interactions where the final state of the electron is an unoccupied bound state are also possible. These interactions correspond to Raman scattering (see, for example, Baym 1974), a process that involves relatively small energy transfers and is usually disregarded in high-energy Monte Carlo codes.

Exact non-relativistic DCSs for Compton scattering by hydrogenic ions in the ground state (K shell) and in the first excited level (L shell) have been evaluated by Eisenberger

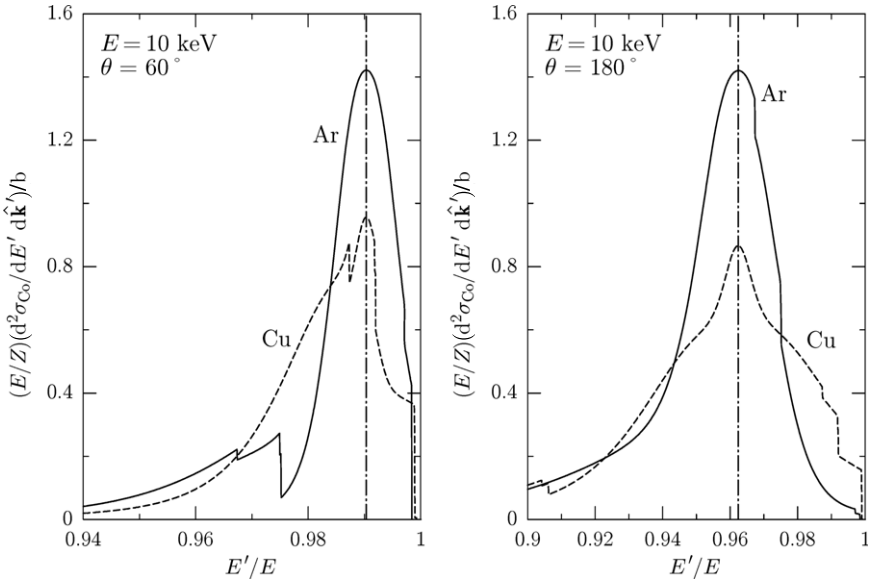

Figure 2. DCSs for Compton scattering of 10 keV photons by free argon and copper atoms at the indicated scattering angles. The dot–dashed vertical line is the Compton line, equation (31).

and Platzman (1970) and by Bloch and Mendelsohn (1974), respectively. Their calculations indicate that the impulse approximation is accurate to within a few per cent for energies of a few tens of keV or larger, except near the ionization thresholds of tightly bound shells.

The atomic DCS for Compton scattering is obtained by adding the contributions from the various electron shells. Compton scattering by molecules is described by means of the additivity approximation, that is, the molecular DCS is estimated as the sum of DCSs of the atoms in a molecule. In the case of condensed media, the Compton profiles of outer shells may differ substantially from the free-atom profiles (see Cooper 1985). Since electrons in these shells have relatively small momenta, they can either be considered free electrons at rest or treated as a free-electron gas. Figure 2 shows DCSs, obtained from the impulse approximation, for scattering of 10 keV photons by isolated argon and copper atoms at scattering angles of 60° and 180°. The finite width of the energy spectrum of scattered photons is caused by Doppler broadening.

It is worth mentioning that various compilations of atomic cross sections for Compton scattering (Berger *et al* 2005, Cullen *et al* 1997) and various Monte Carlo codes still rely on the use of the incoherent scattering function to account for binding effects. In this formalism, which is sometimes referred to as the Waller–Hartree approximation, the DCS is set equal to the Klein–Nishina DCS multiplied by the incoherent scattering function $S(q, Z)$, defined by

$$S(q, Z) = \left\langle \Psi_0 \left| \sum_{i=1}^{Z} \sum_{j=1}^{Z} \exp[\mathrm{i}\boldsymbol{q} \cdot (\boldsymbol{r}_j - \boldsymbol{r}_i)] \right| \Psi_0 \right\rangle - [F(q, Z)]^2, \quad (42)$$

where Ψ_0 is the ground-state atomic wave function. Tabulations of this function, for the elements $Z = 1$ to 100 were compiled by Hubbell *et al* (1975, 1977). As pointed out by Ribberfors and Berggren (1982), the assumptions underlying the Waller–Hartree theory are essentially non-relativistic. These authors also obtain a relativistic expression for the incoherent scattering function in terms of the atomic Compton profile, by integrating the atomic DCS over the energy of the scattered photon.

Figure 3 displays energy DCSs, integrated over directions of the scattered photon, for scattering of 50 keV and 500 keV photons by isolated tungsten atoms. The plotted DCSs were obtained from the impulse approximation, and from the Klein–Nishina formula, equation (32). The most conspicuous feature of the impulse approximation is the absence of a threshold energy in the DCS, which is a direct manifestation of the Doppler broadening. For relatively small energy transfers ($E' \sim E$) the Klein–Nishina DCS increases with the energy of the scattered photon, whereas the energy DCS obtained from the impulse approximation vanishes at $E' = E$ due to the effect of binding. The accuracy of the Klein–Nishina formula improves when the photon energy increases, and when the atomic number decreases.

3.4. Electron–positron pair production

Electron–positron pairs can be created by absorption of a photon in the vicinity of a massive charged particle, a nucleus or an electron, which takes energy and momentum so that these two quantities are conserved. The threshold energy for pair production in the field of a nucleus (assumed of infinite mass) is $2m_ec^2$. When pair production occurs in the field of an electron, the target electron recoils after the event with appreciable kinetic energy; the process is known as 'triplet production' because it causes three visible tracks when observed, for example, in a cloud chamber. If the target electron is at rest, triplet production is only possible for photons with energy larger than $4m_ec^2$.

Pair production and bremsstrahlung emission (section 4.3) are closely related processes, and cross sections from pair

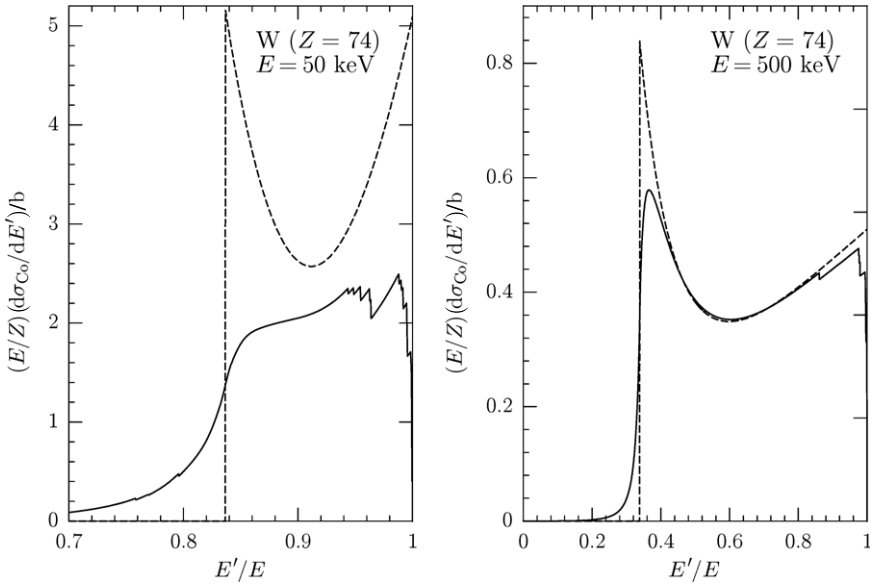

Figure 3. Energy DCSs for Compton scattering of 50 keV and 500 keV photons by free tungsten atoms. The continuous curves represent the DCS obtained from the impulse approximation, by integrating the DCS (34) over directions of the scattered photon. The dashed curves correspond to the Klein–Nishina formula, equation (32) with $E' = E_C$, i.e. they describe collisions with Z electrons free and at rest.

production can be readily obtained from the bremsstrahlung formulae by simple substitutions (see, for example, Akhiezer and Berestetskii 1965, Tsai 1974). Thus, the Bethe–Heitler DCS for pair production (Born approximation) follows from the corresponding DCS for bremsstrahlung emission, equation (98). An extensive list of formulae obtained from the Bethe–Heitler formula, and with more elaborate methods, has been compiled by Motz *et al* (1969).

The process of triplet production differs from that of pair production in the field of the atom in two respects, namely, the possibility of exchange between the two electrons in the final state, and the possibility that the photon be absorbed by the target electron. The transition amplitude for triplet production is given by a complicated analytical expression, which can be deduced from the transition amplitude for electron–electron bremsstrahlung (given by Haug and Nakel 2004). DCSs for triplet production were calculated by Jarp and Mork (1973), who found that for photons with high energies, most of the interactions involve small momentum transfers to the target electron. The total cross section was obtained by Mork (1967).

Let us consider the pair-production process in which an unpolarized incident photon with energy E creates an electron–positron pair in the atomic field. The kinetic energies and momenta of the electron and positron are denoted by $E_-, \hbar\boldsymbol{k}_-$ and $E_+, \hbar\boldsymbol{k}_+$, respectively. As in the case of bremsstrahlung emission, the Born approximation provides a reliable description of the process at high energies. The DCS for pair production is usually expressed as a function of the energy E_+ of the positron and of the directions $\hat{\boldsymbol{k}}_-$ and $\hat{\boldsymbol{k}}_+$ of the pair. Most Monte Carlo codes simulate pair-production events by first sampling the energy of the positron (or the electron) from a theoretical DCSs differential in only the energy of that particle (i.e. using the marginal probability distribution of E_+). Very frequently, the high-energy Bethe–Heitler formula (equation 3D-1003 of Motz *et al* 1969), obtained through an approximate integration of the Born DCS over the directions of the generated pair, is used.

The Bethe–Heitler DCS for a photon of energy E to create an electron–positron pair in the atomic field can be approximated as (Tsai 1974)

$$\frac{\mathrm{d}\sigma_{\mathrm{pp}}^{(\mathrm{BH})}}{\mathrm{d}\epsilon} = r_e^2 Z^2 \left\{ [\epsilon^2 + (1-\epsilon)^2](\Phi_1 - 4f_C) + \frac{2}{3}\epsilon(1-\epsilon)(\Phi_2 - 4f_C) \right\}, \tag{43}$$

where the reduced energy $\epsilon \equiv (E_+ + m_e c^2)/E$ is the fraction of the photon energy carried off by the positron. The screening functions Φ_1 and Φ_2 are given by integrals that involve the atomic form factor and, therefore, must be computed numerically when a realistic form factor is adopted. To obtain approximate analytical expressions for these functions, one may assume that the Coulomb field of the nucleus is exponentially screened by the atomic electrons (Schiff 1951, Tsai 1974), i.e. the electrostatic potential of the atom is represented as

$$\varphi_S(r) = \frac{Ze}{r}\exp(-r/R). \tag{44}$$

The screening radius R is usually chosen to be proportional to the inverse cubic root of the atomic number, $R = aZ^{-1/3}$, in accordance with the Thomas–Fermi model of the atom, with the parameter a determined so as to reproduce, for example, the total cross section obtained from more elaborate calculations. The corresponding atomic electron density is given by Poisson's equation, $\rho_S(r) = (1/4\pi e)\nabla^2\varphi_S(r)$, and the atomic form factor is

$$F_S(q, Z) = 4\pi \int_0^\infty \rho_S(r)\frac{\sin(qr)}{qr} r^2\,\mathrm{d}r = \frac{Z}{1+(Rq)^2}. \tag{45}$$

The screening functions for this particular form factor take the following analytical expressions (Tsai 1974)

$$\Phi_1 = 2 - 2\ln(1+b^2) - 4b\arctan(b^{-1}) + 4\ln(Rm_ec/\hbar),$$
$$\Phi_2 = \frac{4}{3} - 2\ln(1+b^2) + 2b^2[4 - 4b\arctan(b^{-1}) - 3\ln(1+b^{-2})] + 4\ln(Rm_ec/\hbar), \quad (46)$$

where

$$b = \frac{Rm_ec}{\hbar}\frac{m_ec^2}{2E}\frac{1}{\epsilon(1-\epsilon)}. \quad (47)$$

The quantity f_C in equation (43) is the high-energy Coulomb correction of Davies, Bethe and Maximon (1954), which accounts for the effect of the atomic field on the wave functions of the produced particles. Because of the approximate nature of this correction, it should not be used for photon energies of less than about 100 MeV.

The Bethe–Heitler formula (43) yields a DCS for pair production that, considered as a function of the positron reduced energy ϵ, is symmetrical about $\epsilon = 1/2$. This dependence on ϵ is reasonably accurate only for photon energies larger than ∼5 MeV. For lower photon energies, the effect of the electrostatic field of the atom (which slows down the electron and accelerates the positron) becomes increasingly important, with the result that the actual DCS becomes asymmetrical and the mean value of ϵ becomes larger than 1/2 (see, for example, Motz *et al* 1969). At these relatively low energies, however, pair production is not dominant and, moreover, the produced particles have ranges that are much less than the mean free path of the absorbed photon. Therefore, no large simulation errors are introduced by using the Bethe–Heitler DCS, equation (43), for energies down to the threshold.

Cross sections for pair production in the field of a bare point nucleus, i.e. a pure Coulomb field, have been computed by Øverbø *et al* (1973). These authors derived a closed formula for the cross section differential in the energy of the emitted positron, which is given as an infinite series of hypergeometric functions (formula 3D-1006 of Motz *et al* (1969)). This formula yields asymmetric energy spectra for electrons and positrons, but disregards screening effects. Tseng and Pratt (1971a) reported numerical calculations of pair production in screened atomic fields. These calculations are performed by using essentially the same procedure as for the bremsstrahlung process, namely, using the multipole expansion for the photon and the partial-wave expansion in equation (A.13) of the distorted plane waves of the electron and the positron. A review of later work on partial-wave calculations of pair production in screened Coulomb fields has been published by Pratt (2006). Partial-wave calculations are numerically difficult and feasible only for photons with energies up to about $10m_ec^2$, because of the slow convergence of the multipole and partial-wave series. Calculated energy spectra are in fairly good agreement with those obtained from the formula of Øverbø *et al* (1973) for the unscreened Coulomb field.

To complete the simulation of pair-production events, we need to sample the directions of the pair of particles. As the final state involves three bodies (the nucleus and the produced pair), the directions of the produced particles cannot be obtained from only their kinetic energies. The polar angles of the directions of movement of the electron and positron, θ_- and θ_+, relative to the direction of the incident photon are usually sampled from an analytical approximate expression of the DCS, $\mathrm{d}^2\sigma_{\mathrm{pp}}/\mathrm{d}E_\pm\,\mathrm{d}\hat{\boldsymbol{k}}_\pm$, differential in the energy and direction of the particles. The simplest approach is to use the leading term of the high-energy Sauter–Gluckstern–Hull formula for the unscreened point nucleus (equation 3D-2000 in Motz *et al* (1969)), which yields the distribution

$$p(\cos\theta_\pm) = a(1 - \beta_\pm\cos\theta_\pm)^{-2}, \quad (48)$$

where a is a normalisation constant and $\beta_\pm$ are the velocities of the particles in units of the speed of light, see equation (1). A more elaborate approach (Bielajew 1994) uses the high-energy angular distribution for pair production in the screened field (44) derived by Schiff (equation 3D-2003 of Motz *et al* 1969).

Extensive tables of pair-production total cross sections, evaluated by combining different theoretical approximations, have been published by Hubbell *et al* (1980). These tables give the separate contributions of pair production in the field of the nucleus and in that of the atomic electrons for $Z = 1$ to 100 and for photon energies from the threshold up to 10^5 MeV. This is still the most authoritative source of pair-production data available. Hubbell's data are incorporated in the EPDL97 database (Cullen *et al* 1997) and in the XCOM program (Berger *et al* 2005). To our knowledge, in all general-purpose codes, triplet-production events are simulated as if they were pairs.

3.5. Mass attenuation coefficients

The primary quantity for simulating photon histories is the (linear) attenuation coefficient, the reciprocal of the mean free path. It is given by

$$\mu = \mathcal{N}\sigma_{\mathrm{T}}, \quad (49)$$

where $\mathcal{N}$ is the number of atoms (or molecules) per unit volume and $\sigma_{\mathrm{T}} = \sigma_{\mathrm{ph}} + \sigma_{\mathrm{Ra}} + \sigma_{\mathrm{Co}} + \sigma_{\mathrm{pp}}$ is the total interaction cross-section of an atom (or molecule). For a material of mass density ϱ and 'molecular weight' A_{w} (g/mol), $\mathcal{N} = N_{\mathrm{A}}\varrho/A_{\mathrm{w}}$, where N_{A} is Avogadro's number. The dependence of μ on the density of the material is removed by considering the mass attenuation coefficient,

$$\mu/\varrho = (N_{\mathrm{A}}/A_{\mathrm{w}})\sigma_{\mathrm{T}}. \quad (50)$$

To provide a sense of the relative importance of the different interaction processes, figure 4 shows total and partial mass attenuation coefficients of photons in water and lead as functions of the photon energy. These coefficients were obtained from the XCOM program (Berger *et al* 2005), except for the Compton contribution, which was evaluated from the impulse approximation (section 3.3). The plotted mass attenuation coefficient for Rayleigh scattering is obtained from the usual form-factor approximation, i.e. neglecting the anomalous scattering factor in equation (24).

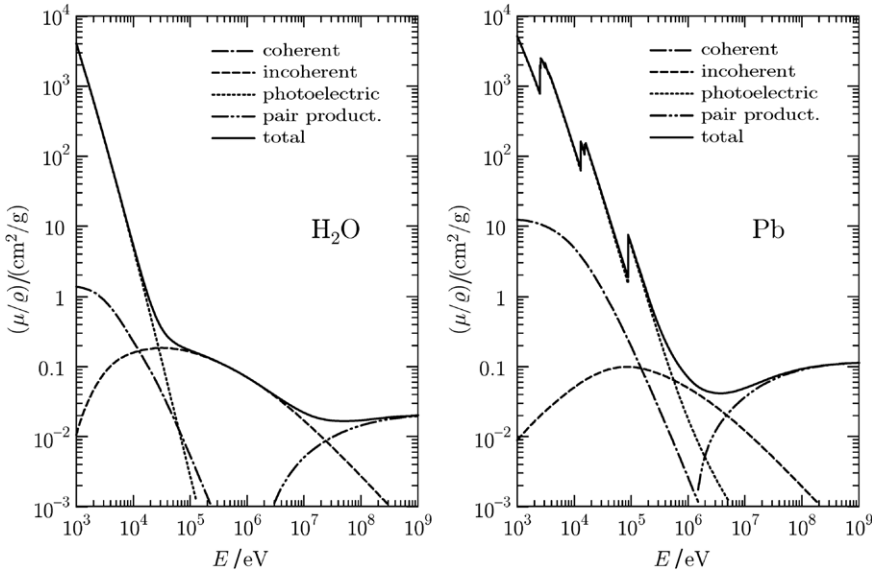

Figure 4. Partial and total mass attenuation coefficients of water and lead as functions of the photon energy.

4. Interactions of electrons and positrons

The dominant interactions of electrons and positrons with atoms are elastic scattering, inelastic collisions and bremsstrahlung emission. Positrons also undergo annihilation, either in flight or at rest. By definition, elastic interactions are those in which the initial and final quantum states of the target atom are the same, normally the ground state. The angular deflections of the trajectories of electrons and positrons in matter are mainly due to elastic scattering; inelastic collisions also cause angular deflections, but these are on average much weaker. Because of the large mass of the nucleus, the recoil energy of the target atom is assumed to be negligible in all interactions.

4.1. Elastic collisions

The theoretical description of elastic collisions is much simpler than that of other collision processes because the effective interaction between the projectile and the atom is essentially electrostatic. Although the nucleus and the atomic electrons have spin magnetic moments, magnetic interactions have a much smaller effect, which can be neglected for most practical purposes. Moreover, it is a good approximation to assume that the charge distribution of the target atom remains frozen in the course of the interaction. This assumption is essentially correct for fast projectiles, with kinetic energies larger than about 10 keV (Salvat 2003). When the projectile is slow, its electric field polarizes the charge distribution of the target atom, and the field of the induced dipole acts back on the projectile. Since the response of the atom is not instantaneous, the atomic polarization sets in only when the electric field applied on the atom varies slowly during a long enough time. That is, only relatively slow projectiles passing at moderate distances from the atom can produce an effective polarization of the latter. Since, in a semiclassical picture, large impact parameters correspond to small scattering angles, the effect of atomic charge polarizability on the elastic-scattering DCSs is limited to relatively small angles (see, for example, ICRU 2007), which are not important for transport studies.

We shall therefore describe elastic collisions on the basis of the so-called *static-field approximation* (Mott and Massey 1965, Walker 1971, ICRU 2007). The interaction energy between the target atom, fixed at the origin of the reference frame, and the projectile is set equal to the (instantaneous) Coulomb interaction energy,

$$V(r) = z_0 e\varphi(r), \tag{51}$$

where $z_0 e$ is the charge of the projectile and $\varphi(r)$ is the electrostatic potential of the target atom (see section 2.1),

$$\varphi(r) = \varphi_{\rm nuc}(r) + \varphi_{\rm el}(r). \tag{52}$$

When the projectile is an electron, the effective interaction is modified by exchange effects, which occur because the projectile is indistinguishable from the atomic electrons. A convenient approach to account for these effects is to add to the 'direct' potential (51) an approximate local-exchange potential,

$$V(r) = -e\varphi(r) + V_{\rm ex}(r). \tag{53}$$

Furness and McCarthy (1973) proposed the following exchange potential,

$$V_{\rm ex}(r) = \frac{1}{2}\left[\frac{\hbar^2 k^2}{2m_{\rm e}} + e\varphi(r)\right] - \frac{1}{2}\left\{\left[\frac{\hbar^2 k^2}{2m_{\rm e}} + e\varphi(r)\right]^2 + 4\pi a_0 e^4 \rho(r)\right\}^{1/2}, \tag{54}$$

where k is the wave number of the projectile electron, equation (2), and $a_0 = \hbar^2/(m_{\rm e}e^2)$ is the Bohr radius. Although the potential (54) is obtained from non-relativistic arguments, it is also approximately valid for relativistic electrons, for which exchange effects are small. Bransden *et al* (1976) have shown

that, for scattering by hydrogen and helium, the potential given by equation (54) describes exchange effects accurately for projectile electrons with kinetic energies larger than about 25 eV.

For simplicity, we consider that incident particles are spin-unpolarized and move in the direction of the positive z axis, and that the final spin state is not observed. Then, the deflection caused by the elastic interaction is characterized by the polar and azimuthal scattering angles θ and ϕ. For a central field, the angular distribution of singly-scattered projectiles is axially symmetric about the direction of incidence, i.e. independent of ϕ. The DCS (per unit solid angle) for elastic scattering of a projectile with kinetic energy E into the solid-angle element $\mathrm{d}\hat{\boldsymbol{k}}'$ about the direction $\hat{\boldsymbol{k}}' = (\theta, \phi)$ is given by (see, for example, Walker 1971, ICRU 2007)

$$\frac{\mathrm{d}\sigma_{\mathrm{el}}}{\mathrm{d}\hat{\boldsymbol{k}}'} = |f(\theta)|^2 + |g(\theta)|^2, \tag{55}$$

where $f(\theta)$ and $g(\theta)$ are the direct and spin-flip scattering amplitudes, which are defined by the partial-wave expansions in equation (A.23*a*) and (A.23*b*). The phase shifts δ_κ (see equation (A.11)) are extracted from the asymptotic behaviour of the numerical solution of the Dirac radial equations (A.5). The DCS, equation (55), accounts for spin and other relativistic effects, as well as for finite nuclear size effects. The Fortran 77 code ELSEPA[1] (Salvat *et al* 2005) calculates scattering amplitudes and DCSs for elastic scattering of electrons and positrons by atoms.

The partial-wave expansions in equation (A.23*a*), (A.23*b*) result from considering the scattering as a stationary process, with the wave function of the projectile described by a distorted plane wave (see the appendix). Alternatively, one could calculate the scattering amplitudes according to equation (A.20). When the distorted plane wave $\psi^{(+)}_{\boldsymbol{k}m_{\mathrm{S}}}(\boldsymbol{r})$ in that expression is replaced by the corresponding plane wave, $\phi_{\boldsymbol{k}m_{\mathrm{S}}}(\boldsymbol{r})$, we obtain the relativistic plane-wave Born approximation (PWBA) to the scattering amplitude matrix,

$$\mathcal{F}^{\mathrm{B}}_{m'_{\mathrm{S}},m_{\mathrm{S}}}(\hat{\boldsymbol{k}}', \hat{\boldsymbol{k}}) = -\frac{4\pi\mathcal{W}}{(c\hbar)^2}\int \phi^{\dagger}_{\boldsymbol{k}'m'_{\mathrm{S}}}(\boldsymbol{r})\, V(r)\, \phi_{\boldsymbol{k}m_{\mathrm{S}}}(\boldsymbol{r})\, \mathrm{d}\boldsymbol{r}. \tag{56}$$

Here we assume that $V(r) = z_0 e\varphi(r)$, that is, in the case of electron scattering we disregard the exchange potential, because exchange effects are negligible when the Born approximation is applicable. Expressing $\mathcal{F}^{\mathrm{B}}(\hat{\boldsymbol{k}}', \hat{\boldsymbol{k}})$ in the form (see equation (A.22))

$$\mathcal{F}^{\mathrm{B}}(\hat{\boldsymbol{k}}', \hat{\boldsymbol{k}}) = \begin{pmatrix} f^{\mathrm{B}}(\theta) & -\mathrm{e}^{-\mathrm{i}\phi} g^{\mathrm{B}}(\theta) \\ \mathrm{e}^{\mathrm{i}\phi} g^{\mathrm{B}}(\theta) & f^{\mathrm{B}}(\theta) \end{pmatrix}, \tag{57}$$

it follows that

$$f^{\mathrm{B}}(\theta) = \left(\frac{\gamma+1}{2} + \frac{\gamma-1}{2}\cos\theta\right) f^{\mathrm{B}}_{\mathrm{n.r.}}(q), \tag{58}$$

$$g^{\mathrm{B}}(\theta) = \frac{\gamma-1}{2}\sin\theta f^{\mathrm{B}}_{\mathrm{n.r.}}(q), \tag{59}$$

[1] The acronym stands for elastic scattering of electrons and positrons by atoms.

where

$$f^{\mathrm{B}}_{\mathrm{n.r.}}(q) \equiv -\frac{m_{\mathrm{e}}}{2\pi\hbar^2}\int V(r)\exp(\mathrm{i}\boldsymbol{q}\cdot\boldsymbol{r})\,\mathrm{d}\boldsymbol{r} \tag{60}$$

is the non-relativistic scattering amplitude (see, for example, Mott and Massey 1965) and $\hbar q = 2\hbar k\sin(\theta/2)$ is the momentum transfer. The Fourier transform of the potential,

$$\mathcal{V}(q) \equiv \int V(r)\exp(\mathrm{i}\boldsymbol{q}\cdot\boldsymbol{r})\,\mathrm{d}\boldsymbol{r}, \tag{61}$$

occurs frequently in calculations within the Born approximation. With the aid of Poisson's equation, $(4\pi e)[\rho_{\mathrm{nuc}}(r) - \rho(r)] = -\nabla^2\varphi(r)$, $\mathcal{V}(q)$ can be transformed into a more familiar form

$$\begin{aligned}\mathcal{V}(q) &= -\frac{z_0 e}{q^2}\int \varphi(r)\nabla^2\exp(\mathrm{i}\boldsymbol{q}\cdot\boldsymbol{r})\,\mathrm{d}\boldsymbol{r} \\ &= -\frac{z_0 e}{q^2}\int [\nabla^2\varphi(r)]\exp(\mathrm{i}\boldsymbol{q}\cdot\boldsymbol{r})\,\mathrm{d}\boldsymbol{r} \\ &= \frac{4\pi z_0 e^2}{q^2}\int [\rho_{\mathrm{nuc}}(r) - \rho(r)]\exp(\mathrm{i}\boldsymbol{q}\cdot\boldsymbol{r})\,\mathrm{d}\boldsymbol{r} \\ &= \frac{4\pi z_0 e^2}{q^2}[F_{\mathrm{nuc}}(q) - F(q, Z)],\end{aligned} \tag{62}$$

where $F(q, Z)$ is the atomic form factor, equation (26), and

$$\begin{aligned}F_{\mathrm{nuc}}(q) &\equiv \int \rho_{\mathrm{nuc}}(r)\exp(\mathrm{i}\boldsymbol{q}\cdot\boldsymbol{r})\,\mathrm{d}\boldsymbol{r} \\ &= \frac{4\pi}{q}\int \rho_{\mathrm{nuc}}(r)\sin(qr)r\,\mathrm{d}r\end{aligned} \tag{63}$$

is the nuclear form factor. Note that for a point nucleus $F_{\mathrm{nuc}}(q) = Z$. Thus, the non-relativistic scattering amplitude can be expressed as

$$f^{\mathrm{B}}_{\mathrm{n.r.}}(q) \equiv -\frac{2m_{\mathrm{e}} z_0 e^2}{(\hbar q)^2}[F_{\mathrm{nuc}}(q) - F(q, Z)]. \tag{64}$$

The DCS for elastic scattering by the potential $V(r)$ obtained from the PWBA is (Mott and Massey 1965)

$$\begin{aligned}\frac{\mathrm{d}\sigma^{\mathrm{B}}}{\mathrm{d}\hat{\boldsymbol{k}}'} &= |f^{\mathrm{B}}(\theta)|^2 + |g^{\mathrm{B}}(\theta)|^2 = \frac{1-\beta^2\sin^2(\theta/2)}{1-\beta^2}|f^{\mathrm{B}}_{\mathrm{n.r.}}(q)|^2 \\ &= \frac{1-\beta^2\sin^2(\theta/2)}{1-\beta^2}\left(\frac{(2m_{\mathrm{e}} z_0 e^2)^2}{(\hbar q)^4}\right) \\ &\quad\times [F_{\mathrm{nuc}}(q) - F(q, Z)]^2.\end{aligned} \tag{65}$$

The quantity in parentheses is the non-relativistic Rutherford DCS, i.e. the DCS for scattering by a bare point nucleus. The factor $[1-\beta^2\sin^2(\theta/2)]/(1-\beta^2)$ arises from relativistic corrections, i.e. spin effects and Lorentz contraction. Finally, the last factor, with the form factors, accounts for the effects of screening of the nuclear charge by the atomic electrons and of the finite size of the nucleus. Note that the PWBA yields the same DCS for electrons and positrons. This approximation is the basis of various calculation models for scattering of electrons and positrons with energies higher than ~10 MeV, where partial-wave methods are impracticable.

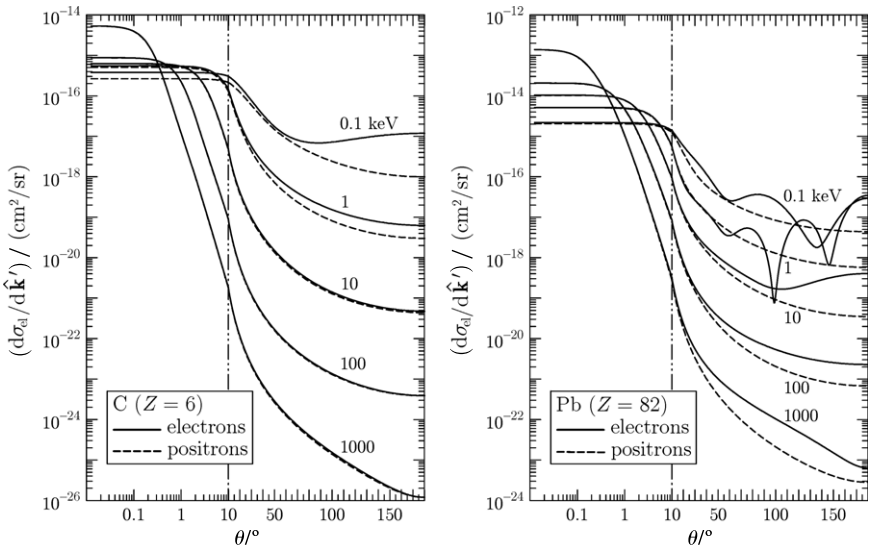

Figure 5. DCSs for elastic scattering of electrons and positrons with the indicated kinetic energies by carbon and lead atoms. Note the logarithmic scale for $\theta < 10^\circ$.

A review of theoretical calculation methods and experimental measurements of elastic scattering of electrons and positrons has recently been published in the ICRU Report 77 (ICRU 2007). This report also includes an extensive database of DCSs for elastic scattering of projectiles with kinetic energies from 50 eV to 100 MeV by atoms of the elements $Z = 1$ to 103, which was generated using the ELSEPA code (Salvat *et al* 2005). Figure 5 displays the DCSs from that database for elastic scattering of electrons and positrons of various energies by atoms of carbon and lead. The plots illustrate the variation of the DCS with the atomic number Z, the charge of the projectile and the energy E. Since the interaction $V(r)$ is attractive for electrons and repulsive for positrons, the scattering is more intense for electrons (which can fall deeply into the potential well of the atom) than for positrons (which are repelled from the nucleus and cannot 'feel' the inner part of the atom). The DCS for low-energy electrons exhibits a diffraction-like structure, while the DCS for positrons decreases monotonically with θ.

4.2. Inelastic collisions

Inelastic collisions of electrons and positrons are usually described by using the first Born approximation (see, for example, Fano 1963). We will sketch the conventional theory to clarify the underlying approximations. For simplicity, we adopt the IPA and use the one-active electron approximation to describe atomic excitations. The interaction between the projectile (0) and the active electron (1) must account for virtual excitations of the electromagnetic field and the Dirac sea (see, for example, Sakurai 1967). When these excitations are described in lowest non-vanishing order of perturbation theory, the effective interaction Hamiltonian takes the form (Fano 1963)

$$\mathcal{H}_{\rm int}(0,1) = -\frac{z_0 e^2}{2\pi^2}\int \mathrm{d}\boldsymbol{q}\left(\frac{1}{q^2} - \frac{\widetilde{\boldsymbol{\alpha}}_0\cdot\widetilde{\boldsymbol{\alpha}}_1 - (\widetilde{\boldsymbol{\alpha}}_0\cdot\hat{\boldsymbol{q}})(\widetilde{\boldsymbol{\alpha}}_1\cdot\hat{\boldsymbol{q}})}{q^2-(W/\hbar c)^2}\right) \times \exp[\mathrm{i}\boldsymbol{q}\cdot(\boldsymbol{r}_1-\boldsymbol{r}_0)], \tag{66}$$

where W is the energy exchanged between the projectile and the target electron. The first term in this expression is the instantaneous (longitudinal) Coulomb interaction. The second term accounts for the exchange of virtual photons and is usually referred to as the transverse interaction.

We assume that before the interaction the projectile moves with velocity $\boldsymbol{v}$, linear momentum $\hbar\boldsymbol{k}$ and kinetic energy E; the corresponding values after the collision are $\boldsymbol{v}'$, $\hbar\boldsymbol{k}'$ and E', respectively. The interaction causes the excitation of the active electron from the initial orbital ψ_a to an unoccupied orbital ψ_b, which can be bound (excitation) or free (ionization). For the sake of brevity, we will limit our considerations to the case of ionization ($W > U_{n_a\kappa_a}$).

Considering the interaction given by equation (66) as a first-order perturbation, the DCS for ionizing collisions is found to be

$$\frac{\mathrm{d}^3\sigma_{\mathrm{in},a}}{\mathrm{d}W\,\mathrm{d}\hat{\boldsymbol{k}}'\,\mathrm{d}\hat{\boldsymbol{k}}_b} = \frac{(2\pi)^4}{\hbar v}k'k_b\frac{E-W+m_\mathrm{e}c^2}{c^2\hbar^2}\frac{E_b+m_\mathrm{e}c^2}{c^2\hbar^2}|T_{fi}|^2, \tag{67}$$

where $W = E - E'$ is the energy loss and $E_b = W - U_{n_a\kappa_a}$ is the kinetic energy of the knock-on electron. The transition matrix element is given by

$$T_{fi} = \langle\psi^{(-)}_{\boldsymbol{k}'m'_\mathrm{s}}(0)\psi_b(1)|\mathcal{H}_{\rm int}(0,1)|\psi^{(+)}_{\boldsymbol{k}m_\mathrm{s}}(0)\psi_a(1)\rangle. \tag{68}$$

In the so-called distorted-wave Born approximation (DWBA), the initial and final states of the projectile are described as distorted plane waves in a certain potential $V(r)$, for instance, the DHFS potential given by equation (11) (Segui *et al* 2003). The DWBA allows taking into account not only the distortion of the projectile waves caused by the atomic potential, but also exchange effects in electron collisions. It also accurately describes differences between DCSs for collisions of electrons and positrons.

For many purposes, only the effect of the interactions on the projectile is of interest, and the relevant DCS is the

integral of expression (67) over the direction $\hat{\boldsymbol{k}}_b$ of the knock-on electron. Usually, the target atoms are randomly oriented, the incident beam is unpolarized and final magnetic and spin states are not distinguished. Under these circumstances, the observed DCS is obtained by averaging over initial degenerate magnetic and spin states and summing over final degenerate states. Following Fano (1963), we introduce the recoil energy Q, defined by

$$Q(Q + 2m_e c^2) = (c\hbar q)^2 = c^2\hbar^2(k^2 + k'^2 - 2kk'\cos\theta), \tag{69}$$

where $\hbar\boldsymbol{q} = \hbar\boldsymbol{k} - \hbar\boldsymbol{k}'$ is the momentum transfer. That is, Q is the kinetic energy of a free electron that moves with momentum $\hbar q$. In the case of binary collisions of the projectile with free electrons at rest we have $Q = W$, because the energy lost by the projectile is equal to the kinetic energy of the recoiling target electron. Noting that

$$\mathrm{d}\hat{\boldsymbol{k}}' = 2\pi\,\mathrm{d}(\cos\theta) = \frac{2\pi(Q + m_e c^2)}{c^2\hbar^2 kk'}\,\mathrm{d}Q, \tag{70}$$

the DCSs for ionization of a closed shell $n_a\ell_a j_a$ can be expressed as

$$\frac{\mathrm{d}^2\sigma_{\mathrm{in},a}}{\mathrm{d}W\,\mathrm{d}Q} = \frac{(2\pi)^5}{c^2\hbar^4 v^2}\frac{E - W + m_e c^2}{E + m_e c^2}(Q + m_e c^2)\mathcal{J}_{fi}, \tag{71}$$

with

$$\mathcal{J}_{fi} \equiv k_b\frac{E_b + m_e c^2}{c^2\hbar^2}\sum_{m_a,m_S}\sum_{m_{Sb},m'_S}\int \mathrm{d}\hat{\boldsymbol{k}}_b |T_{fi}|^2. \tag{72}$$

The DWBA yields reliable results even for projectiles with kinetic energies close to the ionization threshold (Bote and Salvat 2008). Unfortunately, practical computations are difficult and feasible only for energies up to about 20 times the ionization energy $U_{n_a\kappa_a}$ of the active electron shell. To get a more operative form of the theory, the projectile wave functions must be simplified. The PWBA is obtained by replacing the distorted plane waves in the T-matrix elements by plane waves (see equation (A.17)),

$$T_{fi}^{(\mathrm{PWBA})} = \langle\phi_{\boldsymbol{k}'m'_S}(0)\psi_b(1)|\mathcal{H}_{\mathrm{int}}(0,1)|\phi_{\boldsymbol{k}m_S}(0)\psi_a(1)\rangle. \tag{73}$$

The DCS for inelastic collisions of charged particles within the PWBA was first derived by Bethe (1932). An authoritative review of the Bethe theory has been published by Inokuti (1971) (see also Inokuti *et al* 1978). The total DCS for collisions with atoms is obtained by adding the contributions, ionization *and* excitation, of the various electron shells; an average over orbitals of open shells is normally assumed. The atomic DCS for inelastic collisions of a heavy spin-$\frac{1}{2}$ particle with charge $\pm e$ can be expressed as (Fano 1963, Segui *et al* 2002)

$$\frac{\mathrm{d}^2\sigma_{\mathrm{in}}}{\mathrm{d}W\,\mathrm{d}Q} = \frac{2\pi e^4}{m_e v^2}\frac{\mathrm{d}f(Q,W)}{\mathrm{d}W}\left[\frac{1}{WQ(1 + Q/2m_e c^2)} + \frac{\beta_t^2 W/2m_e c^2}{[Q(1 + Q/2m_e c^2) - W^2/2m_e c^2]^2}\right], \tag{74}$$

where the first and second terms in square brackets account for longitudinal and transverse interactions, respectively. The parameter β_t is the component of $\boldsymbol{\beta} = \boldsymbol{v}/c$ perpendicular to $\boldsymbol{q}$,

$$\beta_t^2 = \beta^2 - \frac{W^2}{Q(Q + 2m_e c^2)}\left(1 + \frac{Q(Q + 2m_e c^2) - W^2}{2W(E + m_e c^2)}\right). \tag{75}$$

The key quantity in equation (74) is the generalized oscillator strength (GOS), defined by

$$\frac{\mathrm{d}f(Q,W)}{\mathrm{d}W} \equiv \frac{W}{Q}\frac{2(Q + m_e c^2)}{Q + 2m_e c^2}\sum_{n_a,\kappa_a}\frac{q_a}{2j_a + 1}\frac{k_b}{\pi(E_a + W)} \times \sum_{m_a}\sum_{\kappa_b,m_b}|\langle\psi_{E_b\kappa_b m_b}|\exp(\mathrm{i}\boldsymbol{q}\cdot\boldsymbol{r})|\psi_{n_a\kappa_a m_a}\rangle|^2, \tag{76}$$

where the first summation is over the occupied electron shells $n_a\kappa_a$. Because of the spherical symmetry of closed shells, and the average over orbitals of open shells implicit in equation (76), the GOS is a function of only the energy loss W and the recoil energy Q (i.e. it depends only on the magnitude of the vector $\boldsymbol{q}$). Within the PWBA, the GOS provides a complete description of inelastic collisions of charged particles with atoms.

The PWBA is the basis of the conventional theory of stopping of charged particles (Fano 1963, Inokuti 1971, ICRU 1984). The inelastic collision models used in all high-energy Monte Carlo simulation codes are also based on this approximation. Note that the DCS given by equation (74) describes the effect of the interaction *on the projectile* only. This causes difficulties in determining the initial direction of secondary electrons (delta rays) generated in ionizing collisions. Very frequently, delta rays are assumed to have initial momentum equal to the momentum transfer, which amounts to neglecting binding effects.

Closed analytical formulae for the GOS are available only for the hydrogen atom (see Inokuti 1971). Bote and Salvat (2008) have reported numerical calculations of GOSs for ionization of inner shells of atoms, computed using the DHFS self-consistent potential. The GOS can be represented as a surface over the (Q, W) plane, which is known as the Bethe surface (Inokuti 1971). In the limit of very large recoil energies, the target electrons behave as if they were essentially free and at rest and, consequently, the GOS reduces to a ridge along the line $W = Q$, which was named the Bethe ridge by Inokuti (1971). The GOS satisfies the Bethe sum rule (Inokuti 1971)

$$\int_0^\infty \frac{\mathrm{d}f(Q,W)}{\mathrm{d}W}\,\mathrm{d}W = Z \qquad \text{for any } Q. \tag{77}$$

This sum rule, which is a result from non-relativistic theory (see, for example, Mott and Massey 1965), is assumed to be generally satisfied. It leads to the interpretation of the GOS as the effective number of electrons per unit energy transfer that participate in interactions with given recoil energy Q. The Bethe sum rule also holds for compounds, in which case the quantity Z denotes the number of electrons in a molecule.

The concept of a GOS can be extended to describe inelastic collisions of charged particles in condensed matter (Fano 1963). The main difficulty with this generalization is that the contribution of valence-electron excitations to the GOS depends strongly on the structure of the medium, and its calculation is at present very difficult. In the limit $Q \to 0$, the GOS reduces to the optical oscillator strength (OOS),

$$\frac{\mathrm{d}f(W)}{\mathrm{d}W} \equiv \frac{\mathrm{d}f(Q=0,W)}{\mathrm{d}W}, \tag{78}$$

which is closely related to the (dipole) photoelectric cross-section for photons of energy W and to the optical dielectric function of the medium (Fano 1963). The so-called optical-data models (see, for example, Fernández-Varea *et al* 2005, and references therein) utilize experimental information on optical properties (i.e. the index of refraction and the extinction coefficient) to build the OOS, and generate the GOS (for $Q > 0$) from the OOS by using suitable extension algorithms, usually based on the free-electron-gas theory.

The mean excitation energy I, defined by (Fano 1963, Inokuti 1971)

$$Z \ln I = \int_0^\infty \ln W \frac{\mathrm{d}f(W)}{\mathrm{d}W}\,\mathrm{d}W, \tag{79}$$

plays a central role in the Bethe stopping power formula (see equation (89)). This quantity has been determined empirically for a large number of materials (see ICRU 1984, and references therein) from measurements of the stopping power of heavy charged particles and/or from experimental optical dielectric functions. Most Monte Carlo codes make explicit use of these empirical I values. For materials not included in the ICRU tables, I is usually estimated from the additivity approximation.

The DCS for inelastic collisions with atoms in a condensed medium differs from that of free atoms, equation (74), not only because the corresponding GOS are different but also because of the so-called density effect. The origin of this effect is the polarizability of the medium, which 'screens' the distant transverse interaction causing a net reduction of its contribution to the stopping power. The density effect correction to the stopping power has been studied in detail by Sternheimer (1952) and Sternheimer *et al* (1982). The calculation of the density-effect correction on the DCS for inelastic collisions, using empirical optical-data models of the GOS, is described by Fernández-Varea *et al* (2005). The correction is determined by the OOS, i.e. the GOS contains all the information needed to compute the DCS for electron/positron inelastic interactions in condensed media.

It is worth noting that equation (74) follows from the formulation of Fano (1963), which assumes that $q \ll k$. This assumption is appropriate for heavy projectiles, but not for electrons and positrons, because collisions of these particles may involve momentum transfers comparable to the momentum of the projectile (see below). A more detailed derivation of the DCS for inelastic collisions of electrons and positrons has been described recently by Bote and Salvat (2008). Their result not only generalizes equation (74) for arbitrary momentum transfers but also leads to the definition of a GOS for transverse interactions. In equation (74), this transverse GOS is approximated in terms of the longitudinal GOS, defined by equation (76); the approximation corresponds to equations (21) and (28) in Fano's (1963) review. The same approximation is adopted in semiempirical GOS models for the simulation of inelastic collisions in condensed media (see, for example, Fernández-Varea *et al* 2005, and references therein).

4.2.1. High-Q excitations. As mentioned above, high-Q excitations can be considered as collisions with free electrons at rest ($V = 0$). The DCS obtained from elementary quantum electrodynamics for collisions of two distinguishable electrons (see, for example, Greiner 1994) is the following:

$$\frac{\mathrm{d}^2\sigma^{(\mathrm{free})}}{\mathrm{d}W\,\mathrm{d}Q} = \left(\frac{2\pi z_0^2 e^4}{m_\mathrm{e}v^2}\frac{1}{W^2}\right) F_\mathrm{rel}(W)\delta(Q-W), \tag{80}$$

with

$$F_\mathrm{rel}(W) = 1 - \frac{(2E - W + 4m_\mathrm{e}c^2)W}{2(E+m_\mathrm{e}c^2)^2}. \tag{81}$$

The quantity in parentheses has the same analytical form as the non-relativistic Rutherford energy-loss DCS, but with the relativistic velocity $v = \beta c$ (equation (1)) instead of the non-relativistic speed $v_\mathrm{n.r.} = \sqrt{2E/m_\mathrm{e}}$. The factor $F_\mathrm{rel}(W)$ accounts for other relativistic corrections.

When the projectile is an electron, the DCS for close binary collisions must be corrected to account for the indistinguishability of the projectile and the target electrons. For low-Q (distant) interactions, the effect of this correction is small and can be neglected. The energy-loss DCS for binary collisions of electrons with free electrons at rest, obtained from the Born approximation with proper account of exchange, is given by the Møller (1932) formula,

$$\frac{\mathrm{d}^2\sigma_\mathrm{M}}{\mathrm{d}W\,\mathrm{d}Q} = \frac{2\pi e^4}{m_\mathrm{e}v^2}\frac{1}{W^2}\left[1 + \left(\frac{W}{E-W}\right)^2 - \frac{W}{E-W} + a\left(\frac{W}{E-W} + \frac{W^2}{E^2}\right)\right]\delta(W-Q), \tag{82}$$

where

$$a = \left(\frac{E}{E+m_\mathrm{e}c^2}\right)^2 = \left(\frac{\gamma-1}{\gamma}\right)^2. \tag{83}$$

In the final state we have two indistinguishable free electrons, and it is natural to consider the fastest one as the 'primary'. Accordingly, the maximum allowed energy transfer in close collisions is

$$W_\mathrm{max} = E/2. \tag{84}$$

Positrons do not interact with matter as usual (stable) positively charged particles, because the competing process of annihilation followed by re-creation can cause the same transitions as 'direct' scattering (see, for example, Sakurai 1967). The DCS for binary collisions of positrons with free electrons at rest, obtained from the first Born approximation

including the 'annihilation/creation' mechanism, is given by the Bhabha (1936) formula,

$$\frac{\mathrm{d}^2\sigma_{\mathrm{B}}}{\mathrm{d}W\,\mathrm{d}Q} = \frac{2\pi e^4}{m_{\mathrm{e}}v^2}\frac{1}{W^2}\left[1 - b_1\frac{W}{E} + b_2\left(\frac{W}{E}\right)^2 - b_3\left(\frac{W}{E}\right)^3 + b_4\left(\frac{W}{E}\right)^4\right]\delta(W-Q), \tag{85}$$

where

$$b_1 = \left(\frac{\gamma-1}{\gamma}\right)^2\frac{2(\gamma+1)^2-1}{\gamma^2-1},$$

$$b_2 = \left(\frac{\gamma-1}{\gamma}\right)^2\frac{3(\gamma+1)^2+1}{(\gamma+1)^2},$$

$$b_3 = \left(\frac{\gamma-1}{\gamma}\right)^2\frac{2\gamma(\gamma-1)}{(\gamma+1)^2},$$

$$b_4 = \left(\frac{\gamma-1}{\gamma}\right)^2\frac{(\gamma-1)^2}{(\gamma+1)^2}. \tag{86}$$

Note that the maximum energy loss in collisions of positrons is $W_{\max} = E$.

4.2.2. Collision stopping power. The energy-loss DCS is

$$\frac{\mathrm{d}\sigma_{\mathrm{in}}}{\mathrm{d}W} \equiv \int_{Q_-}^{Q_+}\frac{\mathrm{d}^2\sigma_{\mathrm{in}}}{\mathrm{d}W\,\mathrm{d}Q}\,\mathrm{d}Q, \tag{87}$$

where Q_- and Q_+ are the minimum and maximum kinematically allowed recoil energies, which are given by equation (69) with $\cos\theta = \pm 1$. The collision stopping power S_{col} is defined as the average energy loss per unit path length due to inelastic collisions, and is given by

$$S_{\mathrm{col}} = -\frac{\mathrm{d}E}{\mathrm{d}s} = \mathcal{N}\int_0^{W_{\max}} W\frac{\mathrm{d}\sigma_{\mathrm{in}}}{\mathrm{d}W}\,\mathrm{d}W, \tag{88}$$

where $\mathcal{N}$ is the number of atoms or molecules per unit volume. For projectiles with small and intermediate energies, the integral has to be evaluated numerically. However, when the energy E of the projectile is much larger than the ionization energies of the atomic electrons, the stopping power is given by the celebrated Bethe formula. The derivation of this formula is described by Fano (1963). The contribution of interactions with small and intermediate energy losses can be evaluated analytically by making explicit use of the Bethe sum rule, equation (77). For large W, the energy-loss DCS is approximated by the analytical formulas given above for collisions with free electrons at rest. The Bethe formula can be expressed as

$$S_{\mathrm{col}} = \mathcal{N}\frac{2\pi e^4}{m_{\mathrm{e}}v^2}Z\left\{\ln\left(\frac{E^2}{I^2}\frac{\gamma+1}{2}\right) + f^{(\pm)}(\gamma) - \delta_{\mathrm{F}}\right\}, \tag{89}$$

where I is the mean excitation energy, given by equation (79), and

$$f^{(-)}(\gamma) = 1 - \beta^2 - \frac{2\gamma-1}{\gamma^2}\ln 2 + \frac{1}{8}\left(\frac{\gamma-1}{\gamma}\right)^2 \tag{90}$$

and

$$f^{(+)}(\gamma) = 2\ln 2 - \frac{\beta^2}{12}\left[23 + \frac{14}{\gamma+1} + \frac{10}{(\gamma+1)^2} + \frac{4}{(\gamma+1)^3}\right] \tag{91}$$

for electrons and positrons, respectively.

The quantity δ_{F} is the Fermi density-effect correction to the stopping power (Sternheimer 1952, Sternheimer *et al* 1982). It can be computed from the OOS as (Fano 1963)

$$\delta_{\mathrm{F}} \equiv \frac{1}{Z}\int_0^\infty \frac{\mathrm{d}f(W)}{\mathrm{d}W}\ln\left(1+\frac{L^2}{W^2}\right)\mathrm{d}W - \frac{L^2}{\Omega_{\mathrm{p}}^2}\left(1-\beta^2\right), \tag{92}$$

where L is a real-valued function of β^2 defined as the positive root of the following equation (Inokuti and Smith 1982):

$$\mathcal{F}(L) \equiv \frac{1}{Z}\Omega_{\mathrm{p}}^2\int_0^\infty \frac{1}{W^2+L^2}\frac{\mathrm{d}f(W)}{\mathrm{d}W}\,\mathrm{d}W = 1-\beta^2. \tag{93}$$

The function $\mathcal{F}(L)$ decreases monotonically with L, and hence, the root $L(\beta^2)$ exists only when $1-\beta^2 < \mathcal{F}(0)$; otherwise it is $\delta_{\mathrm{F}} = 0$. Therefore, the function $L(\beta^2)$ starts with zero at $\beta^2 = 1-\mathcal{F}(0)$ and grows monotonically with increasing β^2. Tables of the density-effect correction δ_{F} for many materials (elements and compounds) are given in ICRU (1984).

Figure 6 displays collision stopping powers of electrons in solid aluminium and gold calculated from the optical-data model of Fernández-Varea *et al* (2005), and from the Bethe formula, equation (89), with the mean excitation energy I obtained from the OOS used in the optical-data model calculation. Optical-data models provide quite reliable values of S_{col} for energies down to about 100 eV, as evidenced by the relative agreement with available measurements. It is striking that the 'asymptotic' Bethe formula is in fact valid down to fairly small energies, of the order of 10 keV for high-Z materials; it also accounts for the differences between the stopping powers of electrons and positrons. This formula was used to generate the tables of collision stopping powers of electrons and positrons in ICRU (1984).

In principle, the simulation of individual inelastic collisions should be performed by sampling the energy loss W and the scattering angle (or the recoil energy Q) of the projectile from the DCS given by equation (74). In practice, however, this procedure is too involved, and most Monte Carlo codes have recourse to condensed or mixed simulation schemes (Berger 1963). In mixed schemes, the collective effect of soft interactions (with W less than a certain cutoff value W_{c}) is described as a continuous-slowing-down process, while hard interactions are frequently simulated from the DCSs for collisions with free electrons at rest (i.e. ignoring the effect of electron binding). It is fortunate that multiple scattering tends to smear out the details of the adopted DCS and, as a consequence, accurate results are obtained by simply ensuring that the stopping power has the right value. Under the conditions of validity of the Bethe formula (89), the stopping power is determined by the mean excitation energy I, which summarizes all the dependence of the collision stopping power on the structure of the material. Of course, uncertainties in this empirical parameter translate to simulation results.

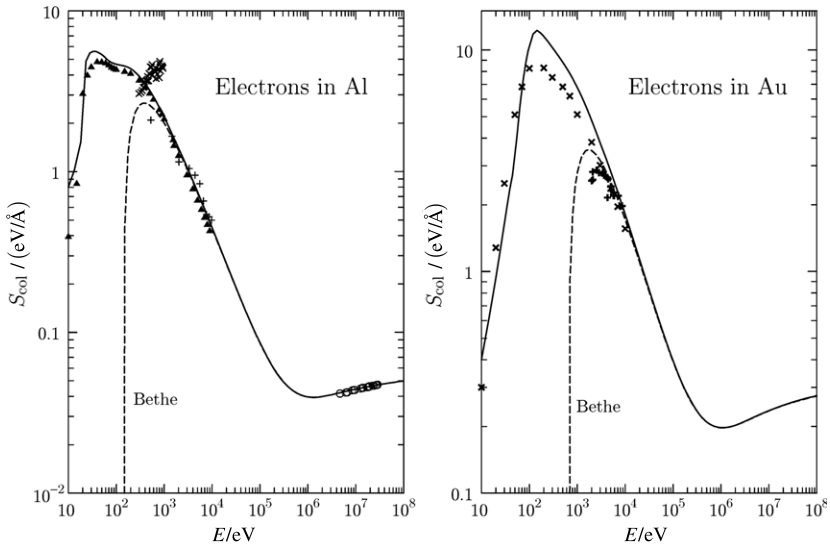

Figure 6. Collision stopping powers for electrons in solid aluminium and gold, as functions of the electron kinetic energy (above Fermi level). The solid curves are theoretical results calculated from the optical-data model of Fernández-Varea *et al* (2005); the symbols are experimental data from various authors. The dashed curves represent collision stopping powers calculated from the Bethe formula, equation (89), with I values derived from the experimental OOS used in the optical-data model calculations.

4.2.3. Ionization of inner shells. To simulate x-ray emission, we need accurate total cross sections for the ionization of individual atomic shells by impact of electrons and positrons. Scofield (1978) calculated cross sections for the ionization of K and L shells of selected elements using the PWBA. However, this approximation yields reliable cross sections only for projectiles with kinetic energies larger than about 30 times the ionization energy of the active shell. A number of approximations based on the PWBA have been proposed, usually by combining analytical approximate forms of the GOS with phenomenological low-energy Coulomb and exchange corrections (Hippler 1990, Deutsch *et al* 1998, Kim *et al* 2000). The Weizsäcker–Williams method of virtual quanta used by Kolbenstvedt (1967) and Seltzer (1988) can also be regarded as a simplification of the PWBA (see, for example, Mayol and Salvat 1990). The most elaborate theoretical calculations of inner-shell ionization by particle impact is provided by the DWBA, but calculations can be performed only for projectiles with kinetic energies up to about $20U_{nK}$.

Bote and Salvat (2008) used the DWBA to evaluate Coulomb and exchange corrections to the PWBA, and generated a database of ionization cross sections for the K, L and M shells of the elements with $Z = 1$ to 99 and for electrons and positrons extending from threshold up to 10^9 eV. Comparison with available experimental data indicates that the calculated cross sections are reliable even for near-threshold energies. Figure 7 shows cross sections from Bote and Salvat's database for ionization of the various shells of the elements argon and tungsten by electron impact. Cross sections obtained from the PWBA are also displayed, to exemplify the domain of validity of this approximation.

4.3. Bremsstrahlung emission

Bremsstrahlung emission by electrons and positrons can occur in the electrostatic field of the atom or in collisions with atomic electrons. Whereas the nuclear recoil has a negligible effect and can be ignored (except at very high energies and large photon emission angles), the recoil of the target electron cannot be neglected, because it affects the kinematics of the process. Moreover, in electron–electron collisions, exchange effects occur. The book of Haug and Nakel (2004) is an excellent review of the theory and experimental measurements of bremsstrahlung emission (see also Haug (2006, 2008)).

A reliable description of bremsstrahlung emission in collisions of electrons and positrons with free electrons is obtained by using the methods of quantum electrodynamics (Haug 2006) with electron states represented by plane waves. The transition matrix element is difficult to calculate, because eight different Feynman diagrams contribute to the transition amplitude. The squared transition matrix element for electron–electron bremsstrahlung, averaged over initial spin states of the electrons and summed over final electron spin states and polarization states of the emitted photon, is given by a very long formula, which can be found in appendix B of Haug and Nakel's book (almost six pages for a single analytical expression). This formula is in covariant form and depends on five invariants. The corresponding average squared matrix element for positron–electron bremsstrahlung can be obtained from that of the electron–electron process by a simple substitution rule (Haug and Nakel 2004). A striking difference between electron–electron and electron–nucleus bremsstrahlung is found in the angular distributions of emitted photons. Whereas the angular distribution of the emitted photon in electron–nucleus (and also in positron–electron) bremsstrahlung is essentially a boosted dipole distribution, the angular distribution of electron–electron bremsstrahlung is quadrupolar (Haug and Nakel 2004). The difference is due to the fact that the electron–electron system has a null electric dipole moment.

The emission of bremsstrahlung in the field of bound electrons can be described by using the impulse approximation

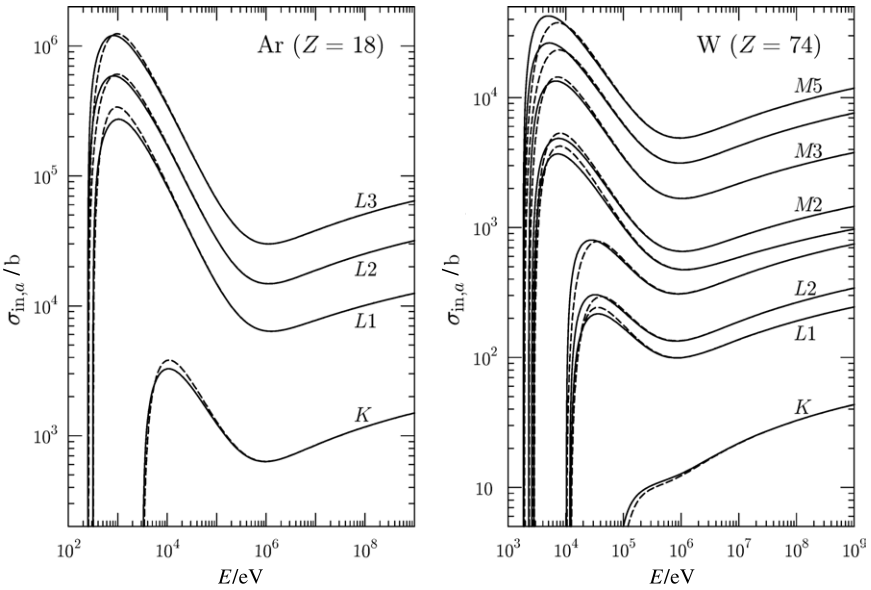

Figure 7. Electron-impact ionization cross sections for K, L and M shells of argon and tungsten. The continuous curves are results from DWBA calculations by Bote and Salvat (2008); dashed curves represent cross sections obtained from the PWBA.

(Haug and Keppler 1984). Alternatively, one may account for the effect of binding (partially disregarding the motion of the target electrons) by using the approximation of Wheeler and Lamb (1939), where binding effects are introduced by simply multiplying the DCS for a target electron free and at rest by the incoherent scattering function $S(q, Z)$, equation (42), where $\hbar q$ is the momentum transfer to the target electron. Seltzer and Berger (1985) used the Wheeler–Lamb approximation to derive a binding correction, which they added to the DCS of free electrons at rest to obtain the total DCS, differential in only the energy of the emitted photon, for bremsstrahlung emission in the field of the atomic electrons. More recently, Tessier and Kawrakow (2008) reported more elaborate calculations of atomic cross sections for electron–electron bremsstrahlung using the Wheeler–Lamb approximation.

Let us now consider the process of electron–nucleus bremsstrahlung in which a free electron with initial kinetic energy E_1 and momentum $\hbar\boldsymbol{k}_1$ is scattered by the electrostatic field of an atom, i.e. by the Coulomb field of the nucleus screened by the atomic electrons. In the interaction, a photon with energy $W = \hbar\omega$ and momentum $\hbar\boldsymbol{k}$ is emitted and thereby the electron jumps to a state with kinetic energy $E_2 = E_1 - W$ and momentum $\hbar\boldsymbol{k}_2$. It is assumed that the mass of the nucleus is much larger than that of the electron, so that it can take arbitrary amounts of recoil momentum and negligible energy. Hence, the final directions of the electron and the emitted photon are independent. Within the formalism of the Furry picture, the DCS for this process, to lowest order, is given by (Tseng and Pratt 1971b)

$$\frac{\mathrm{d}^3\sigma_{\mathrm{br}}}{\mathrm{d}W\,\mathrm{d}\hat{\boldsymbol{k}}\,\mathrm{d}\hat{\boldsymbol{k}}_2} = (2\pi)^2\alpha\frac{W(E_1+m_\mathrm{e}c^2)c\hbar k_2(E_2+m_\mathrm{e}c^2)}{(c\hbar)^4 c\hbar k_1} \times{\sum}' |(M^\dagger_{k\alpha})_{21}|^2, \tag{94}$$

where α is the fine-structure constant. The matrix element is between free-electron states, described by distorted plane waves,

$$(M^\dagger_{k\alpha})_{21} = \left\langle \psi^{(-)}_{\boldsymbol{k}_2,m_{S2}} \middle| \hat{\boldsymbol{\epsilon}}^*_\alpha \cdot \tilde{\boldsymbol{\alpha}} \exp(-\mathrm{i}\boldsymbol{k}\cdot\boldsymbol{r}) \middle| \psi^{(-)}_{\boldsymbol{k}_1,m_{S1}} \right\rangle. \tag{95}$$

We are assuming that the incident electron is unpolarized and that its final spin state and the polarization of the emitted photon are not observed. The primed summation symbol in expression (94) indicates a sum over final electron spin states and photon polarizations, and an average over initial spin states.

Usually, in Monte Carlo calculations it is assumed that deflections of electron trajectories are completely accounted for by the elastic DCS and, consequently, the adopted DCS for bremsstrahlung emission are integrated over the final direction of the projectile electron,

$$\frac{\mathrm{d}^2\sigma_{\mathrm{br}}}{\mathrm{d}W\,\mathrm{d}\hat{\boldsymbol{k}}} = \int \frac{\mathrm{d}^3\sigma_{\mathrm{br}}}{\mathrm{d}W\,\mathrm{d}\hat{\boldsymbol{k}}\,\mathrm{d}\hat{\boldsymbol{k}}_2}\,\mathrm{d}\hat{\boldsymbol{k}}_2. \tag{96}$$

Calculations become much simpler after integrating over $\mathrm{d}\hat{\boldsymbol{k}}$, because angular integrals are performed analytically and each of them effectively removes a large number of terms from the partial-wave series. The energy-loss DCS, differential in only the energy loss (or the energy of the emitted photon) is

$$\frac{\mathrm{d}\sigma_{\mathrm{br}}}{\mathrm{d}W} = \int \frac{\mathrm{d}^2\sigma_{\mathrm{br}}}{\mathrm{d}W\,\mathrm{d}\hat{\boldsymbol{k}}}\,\mathrm{d}\hat{\boldsymbol{k}} \equiv \frac{Z^2}{\beta^2}\frac{1}{W}\chi(Z, E_1, \kappa). \tag{97}$$

The last expression defines the scaled DCS, $\chi(Z, E_1, \kappa)$, as a function of the atomic number Z, the energy of the projectile E_1 and the reduced energy of the photon, $\kappa \equiv W/E_1$. For a given element, this function varies smoothly with E_1 and κ and is therefore amenable for numerical interpolation. Pratt *et al* (1977) produced a table of bremsstrahlung energy spectra for electrons, calculated according to equation (97) using the partial-wave expansion of the distorted plane waves

(equation (A.13)), for all elements and electron kinetic energies from 1 keV to 2 MeV.

Partial-wave DCSs are available only for a limited range of kinetic energies and, therefore, analytical approximate formulae have to be employed for higher energies. The usual practice in Monte Carlo simulation is to rely on the DCS obtained from the first Born approximation (see, for example, Haug and Nakel 2004), which is given by the Bethe–Heitler formula. The calculation is not trivial, because it requires building free-electron wave functions accurate to first order in αZ. Replacing the distorted waves by pure plane waves would yield a null cross section, reflecting the fact that the emission of bremsstrahlung is possible only in the presence of an external particle (potential) which can absorb momentum. After a lengthy derivation, which involves the calculation of traces of products of Dirac matrices using energy-projection operators, one arrives at the Bethe–Heitler formula for the triply DCS (equation 1BS in Koch and Motz (1959)). This important formula is the basis of various approximations used for sampling high-energy bremsstrahlung and pair-production events. To express the Bethe–Heitler DCS, it is convenient to orient the coordinate axes in such a way that the z axis has the direction of $\boldsymbol{k}$, and the momentum of the incident electron lies in the $x-z$ plane, that is,

$$\hat{\boldsymbol{k}} = (0,0,1), \qquad \hat{\boldsymbol{k}}_1 = (\sin\theta_1, 0, \cos\theta_1),$$
$$\hat{\boldsymbol{k}}_2 = (\sin\theta_2\sin\phi, \sin\theta_2\cos\phi, \cos\theta_2).$$

The Bethe–Heitler formula reads

$$\frac{\mathrm{d}^3\sigma_{\mathrm{br}}}{\mathrm{d}W\,\mathrm{d}\hat{\boldsymbol{k}}\,\mathrm{d}\hat{\boldsymbol{k}}_2} = \frac{r_\mathrm{e}^2}{4\pi^2}\frac{p_2 m_\mathrm{e}^2 c^4}{W k_1 q^4}$$
$$\times\left\{[4\mathcal{W}_2^2 - (c\hbar q)^2]\frac{(c\hbar k_1)^2\sin^2\theta_1}{(\mathcal{W}-c\hbar k_1\cos\theta_1)^2}\right.$$
$$+[4\mathcal{W}_1^2-(c\hbar q)^2]\frac{(c\hbar k_2)^2\sin^2\theta_2}{(\mathcal{W}_2-c\hbar k_2\cos\theta_2)^2}$$
$$-[4\mathcal{W}_1\mathcal{W}_2-(c\hbar q)^2+2W^2]$$
$$\times\frac{2(c\hbar)^2k_1k_2\sin\theta_1\sin\theta_2\cos\phi}{(\mathcal{W}_1-c\hbar k_1\cos\theta_1)(\mathcal{W}_2-c\hbar k_2\cos\theta_2)}$$
$$\left.-2W^2\frac{(c\hbar k_1)^2\sin^2\theta_1+(c\hbar k_2)^2\sin^2\theta_2}{(\mathcal{W}_1-c\hbar k_1\cos\theta_1)(\mathcal{W}_2-c\hbar k_2\cos\theta_2)}\right\}$$
$$\times[F_{\mathrm{nuc}}(q)-F(q,Z)]^2, \tag{98}$$

where $\mathcal{W}_i = E_i + m_\mathrm{e}c^2$ are the total energies of the electron and $\hbar q$ is the momentum transferred to the nucleus ($\boldsymbol{q} = \boldsymbol{k}_1 - \boldsymbol{k}_2 - \boldsymbol{k}$),

$$(c\hbar q)^2 = 2W\{[\mathcal{W}_1 - (c\hbar k_1)\cos\theta_1]$$
$$-[\mathcal{W}_2-(c\hbar k_2)\cos\theta_2]\}$$
$$+2[\mathcal{W}_1\mathcal{W}_2-(c\hbar)^2k_1k_2(\cos\theta_1\cos\theta_2$$
$$+\sin\theta_1\sin\theta_2\cos\phi)-m_\mathrm{e}^2c^4]. \tag{99}$$

The form factors $F_{\mathrm{nuc}}(q)$ and $F(q,Z)$ arise through the Fourier transform of the screened potential, $\mathcal{V}(q)$ (see equation (62)), which appears at an intermediate stage in the calculation as a global factor of the transition matrix elements. The nuclear form factor accounts for the effect of the nuclear charge distribution. Usually, a point nucleus is assumed, in which case $F_{\mathrm{nuc}}(q) = Z$. The atomic form factor accounts for the screening of the nuclear charge by the atomic electrons.

A high-energy Coulomb correction, which approximately corrects for the effect of treating the interaction of the projectile with the atomic field as a perturbation, was derived by Davies *et al* (1954). A refined Coulomb correction is described by Seltzer and Berger (1985). Haug (2008) has recently proposed an approximate theory that combines the DCS for the unscreened point nucleus with a screening correction obtained from the Born approximation. The DCS for the nucleus is calculated by using approximate Sommerfeld–Maue wave functions, which are more accurate than the modified plane waves adopted in the Born approximation. The fact that Haug's cross section is given by analytical, although fairly lengthy formulae makes it attractive to improve simulations of electron and positron transport at intermediate energies, at which partial-wave calculations are not feasible.

The Bethe–Heitler DCS is still too complicated to be used in Monte Carlo codes. The usual practice to simulate bremsstrahlung events is to sample first the energy W of the emitted photon from the scaled DCS, $\chi(Z, E_1, \kappa)$ (equation (97)), which is the marginal probability distribution of W. Seltzer and Berger (1985, 1986) have prepared extensive tables of bremsstrahlung energy spectra, obtained by combining different theoretical models, for electrons with kinetic energies E_1 from 1 keV to 10 GeV incident on neutral atoms of the elements $Z = 1$ to 100. These tables include energy spectra for both electron–nucleus and electron–electron bremsstrahlung emission. The DCS for electron–nucleus bremsstrahlung DCS was calculated by combining analytical high-energy theories with results from partial-wave calculations by Pratt *et al* (1977) for bremsstrahlung emission in screened atomic fields and energies below 2 MeV. Seltzer and Berger's tables constitute the most reliable theoretical representation of bremsstrahlung energy spectra available at present, and they are adopted in many Monte Carlo codes. The radiative stopping power of electrons in a single-element medium is calculated from the tabulated scaled DCS as

$$S_{\mathrm{rad}} = \mathcal{N}\int W\frac{\mathrm{d}\sigma_{\mathrm{br}}}{\mathrm{d}W}\,\mathrm{d}W = \mathcal{N}\frac{Z^2}{\beta^2}\int\chi(Z,E_1,\kappa)\,\mathrm{d}W, \tag{100}$$

where $\mathcal{N}$ is the number of atoms per unit volume. Tables of radiative stopping powers, obtained from Seltzer and Berger's scaled DCSs, are given in the ICRU Report 37 (1984).

To complete the simulation of bremsstrahlung emission events, the direction of the emitted photon has to be sampled according to the DCS, equation (96), with W equal to the sampled photon energy. The angular distribution of emitted photons in electron–nucleus bremsstrahlung (the so-called shape function) has been calculated by Kissel *et al* (1983), using the partial-wave expansion method (i.e. from the DCS given by equation (94)), for 144 combinations of atomic number Z, electron energy E_1 and reduced photon energy κ. Acosta *et al* (2002) found that these shape functions can be closely approximated as Lorentz-boosted dipole distributions, from which the emission angle can be sampled analytically.

For energies above 500 keV, the highest energy in the tables of Kissel *et al*, the shape function can be be obtained from the Bethe–Heitler formula (98), or from a suitable approximation to it. Bielajew *et al* (1989) described an analytical method for sampling the photon direction from the Schiff (1951) DCS (equation (2BS) of Koch and Motz 1959). This DCS is obtained from equation (98), through a number of approximations: high-energy limit ($\mathcal{W}, \mathcal{W}_1, W \gg m_e c^2$), exponential screening [$V(r) = -(Ze^2/r)\exp(-r/R)$], small angles and an approximate integration over the scattered electron direction.

To our knowledge, all Monte Carlo codes simulate electron–electron bremsstrahlung by assuming that the angular distribution is the same as for electron–nucleus bremsstrahlung. Also, an important simplification is introduced in the simulation of bremsstrahlung emission by positrons. The scaled cross section for positrons reduces to that of electrons in the high-energy limit, where the Bethe–Heitler formula is applicable, but it is smaller for intermediate and low energies. Cross sections for bremsstrahlung emission by positrons have been calculated by Kim *et al* (1986) using partial-wave methods. These authors found that the ratio of the radiative stopping powers for positrons and electrons can be approximated as a function only of the variable E_1/Z^2, $F_p(E_1/Z^2)$. Because of the lack of more accurate calculations, various codes use DCSs for positrons obtained by multiplying the electron DCS by the scaling factor $F_p(E_1/Z^2)$,

$$\frac{d\sigma_{br}^{(+)}}{dW} = F_p(E_1/Z^2)\frac{d\sigma_{br}^{(-)}}{dW}. \tag{101}$$

The angular distribution of bremsstrahlung photons emitted by positrons is assumed to be the same as for electrons.

4.4. Positron annihilation

Positrons can annihilate with the electrons in the medium by emission of photons. The basic theory of the process is described in Heitler's (1984) book. In the case of annihilation with a free electron, conservation of energy and momentum implies that annihilation can only happen with emission of at least two photons. Indeed, the dominant process is that of two-photon annihilation; the probability of annihilation with emission of three or more photons is about 400 times smaller. When the target electron is bound to an atom, annihilation can occur with emission of only one photon, but the probability is again considerably smaller, by a factor of the order of $(\alpha Z)^4$, than for two-photon annihilation (Broda and Johnson 1972, Tseng and Pratt 1973). It is also possible that, after slowing down, the positron forms a positronium atom before annihilating (see Heitler 1984). When the atom is in the singlet ^{1}S state, annihilation occurs with emission of two quanta. From the triplet ^{3}S state, the atom must annihilate with emission of, at least, three photons. The probability of three-photon annihilation is about 400 times smaller than for two-photon decay.

In most Monte Carlo codes, positron annihilation is described by assuming that the target electrons are free and at rest, thus disregarding electron binding effects, and considering only two-photon emission. The DCS (per electron) for two-photon annihilation, as observed in the centre-of-mass system of the positron and the electron, is derived by Heitler (1984), Nelson *et al* (1985) transformed this DCS to the laboratory system (where the electron is at rest). Let us consider the annihilation of a positron with kinetic energy E via emission of two photons with energies E_+ and E_-, which add to $E+2m_e c^2$. Quantities referring to the photon with the lowest energy will be denoted by the subscript ' $-$ '. Each annihilation event is then completely characterized by the quantity

$$\zeta \equiv \frac{E_-}{E + 2m_e c^2}. \tag{102}$$

If the positron moves initially in the direction of the z-axis, from conservation of energy and momentum it follows that the two photons are emitted in directions with polar angles

$$\cos\theta_- = (\gamma^2 - 1)^{-1/2}(\gamma + 1 - 1/\zeta) \tag{103}$$

and

$$\cos\theta_+ = (\gamma^2 - 1)^{-1/2}[\gamma + 1 - 1/(1-\zeta)], \tag{104}$$

which are determined by ζ. The maximum value of ζ is 1/2, its minimum value is found when $\cos\theta_- = -1$ and is given by

$$\zeta_{min} = [\gamma + 1 + (\gamma^2 - 1)^{1/2}]^{-1}. \tag{105}$$

The DCS for annihilation by an electron at rest is (Nelson *et al* 1985)

$$\frac{d\sigma_{an}}{d\zeta} = \frac{\pi r_e^2}{(\gamma+1)(\gamma^2-1)}[S(\zeta) + S(1-\zeta)], \tag{106}$$

where

$$S(\zeta) = -(\gamma+1)^2 + (\gamma^2 + 4\gamma + 1)\frac{1}{\zeta} - \frac{1}{\zeta^2}. \tag{107}$$

For fast positrons, annihilation photons are emitted preferentially at forward directions. When the kinetic energy of the positron decreases, the angular distribution of the generated photons becomes more isotropic. The total cross-section per electron for two-photon annihilation, which is obtained by integrating expression (106) over ζ, decreases monotonically when the energy E of the positron increases. In most cases, a high-energy positron loses practically all its kinetic energy before annihilating.

5. Atomic relaxation

Interactions of photons and electrons that cause the emission of secondary electrons (photoelectric absorption, Compton scattering of photons, inelastic collisions of electrons and positrons, etc) leave the target atom ionized and in an excited state. The excited ion then relaxes to its ground state through a sequence of radiative and non-radiative transitions, in which photons (fluorescence x-rays) and Auger electrons are emitted, respectively. In inelastic collisions of charged particles, and in Compton scattering, shells with larger ionization energies

$U_{n_a\kappa_a}$ have smaller cross sections, and smaller probabilities of being ionized. In the photoelectric effect, however, the shell cross sections increase with $U_{n_a\kappa_a}$ (Cullen *et al* 1997), that is, photons of energy E have a tendency to ionize the innermost possible electron shell with $U_{n_a\kappa_a} < E$.

A comprehensive review of the theory and measurements of fluorescence yields and Auger and Coster–Kronig transition probabilities was published by Bambynek *et al* (1972). Hubbell *et al* (1994, 2004) reviewed fluorescence data and fitted empirical values for the K, L and M shells. More recently, Campbell (2003) has undertaken a critical examination of fluorescence yields and Coster–Kronig probabilities for the atomic L subshells. An extensive tabulation of experimental x-ray energies was produced by Bearden (1967). The most updated compilation of transition energies for K and L x-rays is that of Deslattes *et al* (2003).

Various Monte Carlo codes simulate atomic relaxation using information from the LLNL Evaluated Atomic Data Library (Perkins *et al* 1991), which provides a comprehensive tabulation of transition probabilities and energies for both radiative and non-radiative transitions for all elements. The transition probabilities in this library were calculated theoretically by assuming that the relaxing ion has a single vacancy (an assumption that ceases to hold, for example, after a non-radiative transition) and transition energies were approximated from the shell ionization energies of the neutral atoms. In simulations of x-ray spectra, these simplifications lead to visible inconsistencies. X-ray energies can be readily corrected by using values from Deslattes *et al* (2003) and Bearden (1967).

6. Concluding comments

We would like to conclude by stressing the fact that general-purpose Monte Carlo codes are subject to a compromise between generality and accuracy. The generic interaction models currently in use are certainly incapable of describing the finest details of the interactions in real media. The approximations that plague the models are bound to produce artefacts that become evident in extreme cases, e.g. in transmission through very thin foils or when the emerging radiation is analysed with high energy or angular resolutions. Nevertheless, today's Monte Carlo codes do provide accurate results in many practical applications, primarily because each approximation has only a weak influence on the simulation results.

Various common approximations are likely to be improved in the near future. Better theoretical models are already available, and they have not yet been adopted only because they are not amenable to analytical manipulation. Thus, angular distributions of photoelectrons obtained from partial-wave calculations could be employed, replacing the Sauter distribution, equation (17). In pair production, the energies of the produced particles may be sampled from the distribution of Øverbø *et al* (1973) for pair production in a Coulomb field. Refined cross sections for inelastic collisions of electron and positron inelastic collisions, based on approximate GOS models, can be introduced to allow a more detailed description of secondary-electron emission. Angular distributions of electron–nucleus bremsstrahlung at high energies could be improved by using Haug's (2008) formulation; the angular distribution for electron–electron bremsstrahlung may also be introduced. In the case of positron annihilation, the impulse approximation could be used to account for the motion of the target electrons; one-photon annihilation by bound electrons could also be included.

Acknowledgments

The authors are indebted to David Bote for helping with various parts of the text and with numerical calculations, and to Llorenç Brualla for his critical reading of the manuscript. Financial support from the Spanish Ministerio de Educación y Ciencia (project no FPA2006-12066) and FEDER, and from the Generalitat de Catalunya (SGR 00013) is gratefully acknowledged.

Appendix A. Dirac wave functions

The relativistic wave equation for the electron is the Dirac equation. The Dirac Hamiltonian for an electron in a central field $V(r)$ is (see, for example, Rose 1961, Sakurai 1967)

$$\mathcal{H}_{\mathrm{D}} = c\widetilde{\boldsymbol{\alpha}} \cdot \boldsymbol{p} + \widetilde{\beta} m_{\mathrm{e}} c^2 + V(r), \tag{A.1}$$

where $\boldsymbol{p} = -\mathrm{i}\hbar\nabla$ is the linear momentum operator, and $\widetilde{\boldsymbol{\alpha}}$ and $\widetilde{\beta}$ are the Dirac matrices. The standard (or split) representation of these matrices is

$$\widetilde{\boldsymbol{\alpha}} = \begin{pmatrix} 0 & \boldsymbol{\sigma} \\ \boldsymbol{\sigma} & 0 \end{pmatrix}, \qquad \widetilde{\beta} = \begin{pmatrix} I_2 & 0 \\ 0 & -I_2 \end{pmatrix}, \tag{A.2}$$

where $\boldsymbol{\sigma}$ stands for the familiar 2×2 Pauli spin matrices and I_2 is the 2×2 unit matrix. The time-independent Dirac wave equation has the form

$$[c\widetilde{\boldsymbol{\alpha}} \cdot \boldsymbol{p} + \widetilde{\beta} m_{\mathrm{e}} c^2 + V(r)]\psi(\boldsymbol{r}) = \mathcal{W}\psi(\boldsymbol{r}), \tag{A.3}$$

where $\mathcal{W}$ is the (total) energy eigenvalue.

The total energy $\mathcal{W}$ of a free electron ($V \equiv 0$) can take positive and negative values ($\mathcal{W} \geqslant m_{\mathrm{e}}c^2$, $\mathcal{W} \leqslant -m_{\mathrm{e}}c^2$). Negative-energy states cannot be interpreted on an equal footing as the positive-energy states, because normal electrons in positive-energy states cannot make radiative transitions to negative-energy states. A partial solution is provided by Dirac's 'hole theory', which assumes that negative-energy states are filled with electrons according to Pauli's exclusion principle. Since the *Dirac sea* of negative-energy states cannot accommodate more electrons, the stability of matter is thus assured. However, it is possible for a negative-energy electron to absorb electromagnetic radiation and be excited to a positive-energy state. When this process occurs, we observe an electron of charge $-e$ and positive energy and a hole in the negative-energy sea. The hole reflects the absence of an electron of charge $-e$ and negative energy $-|\mathcal{W}|$ and can be interpreted as the presence of a particle of charge $+e$, mass m_{e} and positive energy $+|\mathcal{W}|$ in the Dirac sea, the positron. This

is the hole-theory description of the electron-positron pair-production process. With the methods of second quantification (Heitler 1984, Sakurai 1967), the theory is formulated in terms of electrons and positrons, avoiding the need of considering the infinite sea of negative-energy electrons.

The angular momentum operator for a Dirac particle is $\boldsymbol{J} = \boldsymbol{L} + \boldsymbol{S}$, where $\boldsymbol{L} = -\mathrm{i}\boldsymbol{r} \times \nabla$ is the orbital angular momentum and $\boldsymbol{S}$ is the spin angular momentum (all angular momenta are in units of $\hbar$). Since $\mathcal{H}_\mathrm{D}$ commutes with $\boldsymbol{J}^2$, J_z and with the parity operator ($\mathcal{P} = \widetilde{\beta}\times$ space inversion), there exists a complete basis of eigenfunctions common to these four operators. For positive-energy states, these eigenfunctions are the spherical waves, and have the form (Rose 1961, Grant 1970)

$$\psi_{E\kappa m}(\boldsymbol{r}) = \frac{1}{r}\begin{pmatrix} P(r)\Omega_{\kappa,m}(\hat{\boldsymbol{r}}) \\ \mathrm{i}Q(r)\Omega_{-\kappa,m}(\hat{\boldsymbol{r}}) \end{pmatrix}, \tag{A.4}$$

where $\Omega_{\kappa,m}(\hat{\boldsymbol{r}})$ are spherical spinors, and $P(r)$ and $Q(r)$ are the large- and small-component radial wave functions, which satisfy the coupled differential equations

$$\begin{aligned} \frac{\mathrm{d}P}{\mathrm{d}r} &= -\frac{\kappa}{r}P + \frac{E - V + 2m_\mathrm{e}c^2}{c\hbar}Q, \\ \frac{\mathrm{d}Q}{\mathrm{d}r} &= -\frac{E - V}{c\hbar}P + \frac{\kappa}{r}Q, \end{aligned} \tag{A.5}$$

where $E = \mathcal{W} - m_\mathrm{e}c^2$ is the electron energy, exclusive of its rest energy. The spherical spinors are eigenfunctions of the total angular momentum in Pauli's theory, and are given by

$$\Omega_{\kappa,m}(\hat{\boldsymbol{r}}) \equiv \sum_{m_\mathrm{S}=\pm 1/2} \langle \ell, 1/2, m - m_\mathrm{S}, m_\mathrm{S} | j, m\rangle Y_{\ell,m-m_\mathrm{S}}(\hat{\boldsymbol{r}})\chi_{m_\mathrm{S}}, \tag{A.6}$$

where the quantities $\langle ....|..\rangle$ are Clebsch–Gordan coefficients, $Y_{\ell m}(\hat{\boldsymbol{r}})$ are spherical harmonics and χ_{m_S} are the unit Pauli spinors. To simplify notation, it is customary to introduce the relativistic angular momentum quantum number

$$\kappa = (\ell - j)(2j + 1), \tag{A.7}$$

which specifies both the total angular momentum [j] and the parity [$(-1)^\ell$] of the Dirac spherical wave,

$$j = |\kappa| - \frac{1}{2}, \qquad \ell = j + \frac{\kappa}{2|\kappa|}. \tag{A.8}$$

The wave functions of negative-energy states can be obtained by applying the charge-conjugation transformation to the positive-energy states of an electron in the potential $-V(r)$ (Rose 1961). In what follows, we consider only positive-energy states.

The potentials occurring in the study of interactions of radiation with atoms are combinations of a short-range field and a Coulomb field,

$$V(r) = V_\mathrm{sr} + \frac{Z_\infty e^2}{r}, \tag{A.9}$$

where the short-range component is assumed to vanish for $r > r_\mathrm{c}$. Thus, for the DHFS field of neutral atoms, equation (11), r_c is the onset of the Latter tail and $Z_\infty = -1$. Radial wave functions for these potentials can be calculated numerically to high accuracy by using the subroutine package RADIAL (Salvat *et al* 1995). The numerical algorithm implemented in these subroutines combines a cubic-spline interpolation of the function $rV(r)$ with local power-series expansions of the radial wave functions in such a way that truncation errors are effectively reduced. In the case of bound orbitals ($E < 0$), each discrete energy level is characterized by the principal quantum number n and the relativistic quantum number κ. For a given n, the allowed values of κ range from $-n$ to $n-1$. Bound orbitals satisfy the orthonormality relation

$$\int \psi^\dagger_{n'\kappa'm'}(\boldsymbol{r})\psi_{n\kappa m}(\boldsymbol{r})\,\mathrm{d}\boldsymbol{r} = \delta_{n'n}\delta_{\kappa'\kappa}\delta_{m'm}. \tag{A.10}$$

The radial wave functions of free spherical waves ($E > 0$) are normalized in such a way that the large-component radial function asymptotically oscillates with unit amplitude,

$$P(r) \underset{r\to\infty}{\sim} \sin\left(kr - \ell\frac{\pi}{2} - \eta\ln(2kr) + \delta_{E\kappa}\right), \tag{A.11}$$

where k, equation (2), is the wave number and $\eta = Z_\infty e^2 m_\mathrm{e}/(\hbar^2 k)$ is the Sommerfeld parameter. The phase shift $\delta_{E\kappa}$ is obtained from the behaviour of the radial function $P(r)$ at large r. Free spherical waves normalized in the form (A.11) satisfy the orthogonality relation

$$\int \psi^\dagger_{E'\kappa'm'}(\boldsymbol{r})\psi_{E\kappa m}(\boldsymbol{r})\,\mathrm{d}\boldsymbol{r} = \frac{\pi(E + m_\mathrm{e}c^2)}{E + 2m_\mathrm{e}c^2}\delta(k' - k)\delta_{\kappa'\kappa}\delta_{m'm}. \tag{A.12}$$

In collision theory, states of free electrons in the initial and final channels are described as distorted plane waves, i.e. by solutions of the Dirac equation for the potential $V(r)$ that asymptotically behave as a plane wave plus an outgoing (+) or incoming (−) spherical wave. A distorted plane wave is characterized by the wave vector $\boldsymbol{k}$ and spin m_S; it can be expanded on the basis of spherical waves as (Rose 1961, Pratt *et al* 1973)

$$\begin{aligned} \psi^{(\pm)}_{\boldsymbol{k}m_\mathrm{S}}(\boldsymbol{r}) = {} & \frac{1}{k}\sqrt{\frac{E + 2m_\mathrm{e}c^2}{\pi(E + m_\mathrm{e}c^2)}} \\ & \times \sum_{\kappa,m} \mathrm{i}^\ell \exp(\pm\mathrm{i}\delta_{E\kappa})\{[\Omega_{\kappa m}(\hat{\boldsymbol{k}})]^\dagger \chi_{m_\mathrm{S}}\}\psi_{E\kappa m}(\boldsymbol{r}), \end{aligned} \tag{A.13}$$

where

$$E = \sqrt{(c\hbar k)^2 + (m_\mathrm{e}c^2)^2} - m_\mathrm{e}c^2 \tag{A.14}$$

is the kinetic energy of the electron. With the adopted normalization for free spherical waves, the distorted plane waves satisfy the orthogonality relation

$$\int \left[\psi^{(\pm)}_{\boldsymbol{k}'m'_\mathrm{S}}(\boldsymbol{r})\right]^\dagger \psi^{(\pm)}_{\boldsymbol{k}m_\mathrm{S}}(\boldsymbol{r})\,\mathrm{d}\boldsymbol{r} = \delta(\boldsymbol{k}' - \boldsymbol{k})\delta_{m'_\mathrm{S}m_\mathrm{S}}. \tag{A.15}$$

The distorted plane waves have the following asymptotic behaviour

$$\psi^{(\pm)}_{\boldsymbol{k}m_\mathrm{S}}(\boldsymbol{r}) \underset{r\to\infty}{\sim} \phi_{\boldsymbol{k}m_\mathrm{S}}(\boldsymbol{r}) + \psi^{(\pm)}_\mathrm{dist}(\boldsymbol{r}), \tag{A.16}$$

where

$$\phi_{\boldsymbol{k}m_S}(\boldsymbol{r}) = \frac{1}{(2\pi)^{3/2}}\exp(\mathrm{i}\boldsymbol{k}\cdot\boldsymbol{r})\sqrt{\frac{E+2m_ec^2}{2E+2m_ec^2}} \times \left(\frac{I_2}{\sqrt{\dfrac{E}{E+2m_ec^2}}\boldsymbol{\sigma}\cdot\hat{\boldsymbol{k}}}\right)\chi_{m_S} \tag{A.17}$$

is a positive-energy plane wave that represents a beam of electrons with momentum $\hbar\boldsymbol{k}$ and spin state χ_{m_S}. The second term in expression (A.16) is an outgoing (+) or incoming (−) spherical wave,

$$\psi^{(\pm)}_{\mathrm{dist}}(\boldsymbol{r}) = \frac{1}{(2\pi)^{3/2}}\frac{\exp(\pm\mathrm{i}kr)}{r}\sqrt{\frac{E+2m_ec^2}{2E+2m_ec^2}} \times \left(\frac{I_2}{\pm\sqrt{\dfrac{E}{E+2m_ec^2}}\boldsymbol{\sigma}\cdot\hat{\boldsymbol{r}}}\right)\mathcal{F}(\pm k\hat{\boldsymbol{r}},\boldsymbol{k})\chi_{m_S}. \tag{A.18}$$

The scattering amplitude $\mathcal{F}(\pm k\hat{\boldsymbol{r}},\boldsymbol{k})$ is a 2×2 matrix,

$$\mathcal{F}(\hat{\boldsymbol{k}}',\hat{\boldsymbol{k}}) = \begin{pmatrix}\mathcal{F}_{1/2,1/2} & \mathcal{F}_{1/2,-1/2}\\ \mathcal{F}_{-1/2,1/2} & \mathcal{F}_{-1/2,-1/2}\end{pmatrix}, \tag{A.19}$$

with elements

$$\mathcal{F}_{m_S',m_S} = -\frac{4\pi\mathcal{W}}{(c\hbar)^2}\int \phi^{\dagger}_{\boldsymbol{k}'m_S'}(\boldsymbol{r})V(r)\psi^{(+)}_{\boldsymbol{k}m_S}(\boldsymbol{r})\,\mathrm{d}\boldsymbol{r}. \tag{A.20}$$

This matrix determines the spin state of electrons in the spherical wave component. In time-dependent perturbation theory, the distorted plane waves $\psi^{(+)}_{\boldsymbol{k}m_S}(\boldsymbol{r})$ and $\psi^{(-)}_{\boldsymbol{k}m_S}(\boldsymbol{r})$ represent electron states in the initial and final channels, respectively (see Breit and Bethe 1954).

The distorted plane wave $\psi^{(+)}_{\boldsymbol{k}m_S}(\boldsymbol{r})$ can be regarded as the wave function of a stationary scattering state, with the emerging spherical wave representing the scattered electron flux. The scattering amplitude matrix can be expressed in a more explicit form by adopting a reference frame with the z-axis along the initial direction, $\hat{\boldsymbol{z}} = \hat{\boldsymbol{k}}$. Then,

$$\hat{\boldsymbol{k}}' = (\sin\theta\cos\phi, \sin\theta\sin\phi, \cos\theta), \tag{A.21}$$

where θ and ϕ are the polar and azimuthal angles of the 'final' direction $\hat{\boldsymbol{k}}'$, respectively. We have

$$\mathcal{F}(\hat{\boldsymbol{k}}',\hat{\boldsymbol{k}}) = \begin{pmatrix}f(\theta) & -\mathrm{e}^{-\mathrm{i}\phi}g(\theta)\\ \mathrm{e}^{\mathrm{i}\phi}g(\theta) & f(\theta)\end{pmatrix}. \tag{A.22}$$

The functions $f(\theta)$ and $g(\theta)$ are called the 'direct' and 'spin-flip' scattering amplitudes, respectively, and are given by the following partial-wave series

$$f(\theta) = \frac{1}{2\mathrm{i}k}\sum_{\ell}\{(\ell+1)[\exp(2\mathrm{i}\delta_{E,\kappa=-\ell-1})-1] + \ell[\exp(2\mathrm{i}\delta_{E,\kappa=\ell})-1]\}P_\ell(\cos\theta), \tag{A.23a}$$

$$g(\theta) = \frac{1}{2\mathrm{i}k}\sum_{\ell}[\exp(2\mathrm{i}\delta_{E,\kappa=\ell}) - \exp(2\mathrm{i}\delta_{E,\kappa=-\ell-1})]P^1_\ell(\cos\theta), \tag{A.23b}$$

where $P_\ell(\cos\theta)$ and $P^1_\ell(\cos\theta)$ are Legendre polynomials and associated Legendre functions, respectively (see, for example, Abramowitz and Stegun 1974). In the limit where the strength of the potential tends to zero ($V = 0$), the phase shifts vanish, the radial functions of free states ($E > 0$) reduce to regular spherical Bessel functions, and the distorted plane waves reduce to plane waves.

References

Abramowitz M and Stegun I A 1974 (eds) *Handbook of Mathematical Functions* (New York: Dover)

Acosta E, Llovet X and Salvat F 2002 Monte Carlo simulation of bremsstrahlung emission by electrons *Appl. Phys. Lett.* **80** 3228–30

Agostinelli S *et al* 2003 Geant4—a simulation toolkit *Nucl. Instrum. Methods* A **506** 250–303

Akhiezer A I and Berestetskii V B 1965 *Quantum Electrodynamics* (New York: Interscience)

Alling W R and Johnson W R 1965 Exact calculation of K-shell and L-shell photoeffect *Phys. Rev.* **139** A1050–62

Allison J *et al* 2006 Geant4 developments and applications *IEEE Trans. Nucl. Sci.* **53** 270–8

Bambynek W, Crasemann B, Fink R W, Freund H-U, Mark H, Swift C D, Price R E and Venugopala Rao P 1972 X-ray fluorescence yields, Auger yields and Coster–Kronig transition probabilities *Rev. Mod. Phys.* **44** 716–813

Bambynek W, Crasemann B, Fink R W, Freund H-U, Mark H, Swift C D, Price R E and Venugopala Rao P 1974 *Rev. Mod. Phys.* **46** 853 (erratum)

Baró J, Sempau J, Fernández-Varea J M and Salvat F 1995 PENELOPE: an algorithm for Monte Carlo simulation of the penetration and energy loss of electrons and positrons in matter *Nucl. Instrum. Methods* B **100** 31–46

Baym G 1974 *Lectures in Quantum Mechanics* (Boulder, CO: Westview Press)

Bearden J A 1967 X-ray wavelengths *Rev. Mod. Phys.* **39** 78–124

Berger M J 1963 Monte Carlo calculation of the penetration and diffusion of fast charged particles *Methods in Computational Physics* vol 1 (New York: Academic) pp 135–215

Berger M J, Hubbell J H, Seltzer S M, Chang J, Coursey J S, Sukumar R and Zucker D S 2005 *XCOM: Photon Cross Sections Database* (Gaithersburg, MD: National Institute of Standards and Technology) http://physics.nist.gov/PhysRefData/Xcom/Text/XCOM.html

Berger M J and Seltzer S M 1988 *Monte Carlo Transport of Electrons and Photons* ed T M Jenkins *et al* (New York: Plenum) chapters 7–9

Berger M J and Wang R 1988 Multiple-scattering angular deflections and energy-loss straggling *Monte Carlo Transport of Electrons and Photons* ed T M Jenkins *et al* (New York: Plenum) chapter 2

Bergstrom P M, Surić T, Pisk K and Pratt R H 1993 Compton scattering of photons from bound electrons: full relativistic independent-particle-approximation calculations *Phys. Rev.* A **48** 1134–62

Bethe H A 1932 Bremsformel für Elektronen relativistischer Geschwindigkeit *Z. Phys.* **76** 293–9

Bhabha H J 1936 The scattering of positrons by electrons with exchange on Dirac's theory of the positron *Proc. R. Soc. (Lond.)* A **154** 195–206

Bielajew A F 1994 *Improved Angular Sampling for Pair Production in the EGS4 Code System* PIRS-0287R1 (Ottawa: National Research Council of Canada)

Bielajew A F, Mohan R and Chui C-S 1989 *Improved Bremsstrahlung Photon Angular Sampling in the EGS4 Code*

System PIRS-0203 (Ottawa: National Research Council of Canada)
Biggs F, Mendelsohn L B and Mann J B 1975 Hartree-Fock Compton profiles for the elements *At. Data Nucl. Data Tables* **16** 201–309
Bloch B J and Mendelsohn L B 1974 Atomic *L*-shell Compton profiles and incoherent scattering factors: theory *Phys. Rev.* A **9** 129–55
Bote D and Salvat F 2008 Calculations of inner-shell ionization by electron impact with the distorted-wave and plane-wave Born approximations *Phys. Rev.* A **77** 042701
Bransden B H, McDowell M R C, Noble C J and Scott T 1976 Equivalent exchange potentials in electron scattering *J. Phys. B: At. Mol. Phys.* **9** 1301–17
Breit G and Bethe H A 1954 Ingoing waves in final state of scattering problems *Phys. Rev.* **93** 888–90
Broda K W and Johnson W R 1972 Single-quantum annihilation of positrons by screened *K*- and *L*-shell electrons *Phys. Rev.* A **6** 1693–702
Brusa D, Stutz G, Riveros J A, Fernández-Varea J M and Salvat F 1996 Fast sampling algorithm for the simulation of photon Compton scattering *Nucl. Instrum. Methods* A **379** 167–75
Campbell J L 2003 Fluorescence yields and Coster–Kronig probabilities for the atomic *L* subshells *At. Data Nucl. Data Tables* **85** 291–315
Carlson T A 1975 *Photoelectron and Auger Spectroscopy* (New York: Plenum)
Condon E U 1930 The theory of complex spectra *Phys. Rev.* **36** 1121–33
Cooper M J 1985 Compton scattering and electron momentum determination *Rep. Prog. Phys.* **48** 415–81
Cromer D T and Liberman D 1970 Relativistic calculation of anomalous scattering factors for x-rays *J. Chem. Phys.* **53** 1891–8
Cullen D E 1989 *Program SCATMAN: A Code Designed to Calculate Photon Coherent Scattering Anomalous Scattering Factors and Cross Sections* UCRL-ID-103422 (Livermore, CA: Lawrence Livermore National Laboratory)
Cullen D E, Hubbell J H and Kissel L 1997 *EPDL97 The Evaluated Data Library, '97 Version* vol 6, rev. 5 *Report* UCRL-50400 (Livermore, CA: Lawrence Livermore National Laboratory)
Davies H, Bethe H A and Maximon L C 1954 Theory of bremsstrahlung and pair production. II. Integral cross section for pair production *Phys. Rev.* **93** 788–95
Desclaux J P 1975 A multiconfiguration relativistic Dirac-Fock program *Comput. Phys. Commun.* **9** 31–45
Desclaux J P 1977 *Comput. Phys. Commun.* **13** 71 (erratum)
Deslattes R D, Kessler E G, Indelicato P, de Billy L, Lindroth E and Anton J 2003 X-ray transition energies: new approach to a comprehensive evaluation *Rev. Mod. Phys.* **75** 36–99
Deutsch H, Becker K and Märk T D 1998 Improved low-energy dependence of calculated cross sections for the K-shell ionization of atoms using the Deutsch–Märk formalism *Int. J. Mass Spectrom.* **177** 47–50
Eisenberger P and Platzman P M 1970 Compton scattering of x rays from bound electrons *Phys. Rev.* A **2** 415–23
Fano U 1963 Penetration of protons, alpha particles and mesons *Ann. Rev. Nucl. Sci.* **13** 1–66
Fernández-Varea J M, Liljequist D, Csillag S, Räty R and Salvat F 1996 Monte Carlo simulation of 0.1–100 keV electron and positron transport in solids using optical data and partial wave methods *Nucl. Instrum. Methods* B **108** 35–50
Fernández-Varea J M, Salvat F, Dingfelder M and Liljequist D 2005 A relativistic optical-data model for inelastic scattering of electrons and positrons in condensed matter *Nucl. Instrum. Methods* B **229** 187–218
Ferrari A, Sala P R, Fassò A and Ranft J 2005 FLUKA: *a Multi-particle Transport Code (Program version 2005)*, CERN-2005-10, INFN/TC-05/11, SLAC-R-773 (Geneva: CERN)
Furness J B and McCarthy I E 1973 Semiphenomenological optical model for electron scattering on atoms *J. Phys. B: At. Mol. Phys.* **6** 2280–91
Grant I P 1970 Relativistic calculations of atomic structures *Adv. Phys.* **19** 747–811
Greiner W and Reinhardt J 1994 *Quantum Electrodynamics* (Berlin: Springer)
Halbleib J A, Kensek R P, Mehlhorn T A, Valdez G D, Seltzer S M and Berger M J 1992 *ITS Version 3.0: the Integrated TIGER Series of Coupled Electron/Photon Monte Carlo Transport Codes, Report* SAND91-1634 (Albuquerque, NM: Sandia National Laboratories)
Haug E 2006 Electron-electron and electron-positron bremsstrahlung *Radiat. Phys. Chem.* **75** 1330–45
Haug E 2008 Bremsstrahlung cross-section with screening and Coulomb corrections at high energies *Radiat. Phys. Chem.* **77** 207–14
Haug E and Keppler M 1984 Bremsstrahlung in the field of bound electrons *J. Phys. B: At. Mol. Phys.* **17** 2075–84
Haug E and Nakel W 2004 *The Elementary Process of Bremsstrahlung* (Singapore: World Scientific)
Heitler W 1984 *The Quantum Theory of Radiation* (New York: Dover)
Henke B L, Gullikson E M and Davis J C 1993 X-ray interactions: photoabsorption, scattering, transmission, and reflection at $E = 50$–$30\,000$ eV, $Z = 1$–92 *At. Data Nucl. Data Tables* **54** 181–342
Hippler R 1990 Plane wave Born calculations of K-shell ionization at low velocities *Phys. Lett.* A **144** 81–5
Hirayama H, Namito Y, Bielajew A F, Wilderman S J and Nelson W R 2006 *The EGS5 Code System* SLAC-R-730, KEK 2005-8 (Menlo Park, CA: Stanford Linear Accelerator Center)
Hofstadter R 1956 Electron scattering and nuclear structure *Rev. Mod. Phys.* **28** 214–54
Hubbell J H 1999 Review of photon interaction cross section data in the medical and biological context *Phys. Med. Biol.* **44** R1–22
Hubbell J H, Gimm H A and Øverbø I 1980 Pair, triplet, and total cross sections (and mass attenuation coefficients) for 1 MeV–100 GeV photons in elements $Z = 1$ to 100 *J. Phys. Chem. Ref. Data* **9** 1023–147
Hubbell J H, Trehan P N, Singh N, Chand B, Mehta D, Garg M L, Garg R R, Singh S and Puri S 1994 A review, bibliography, and tabulation of K, L, and higher atomic shell x-ray fluorescence yields *J. Phys. Chem. Ref. Data* **23** 339–64
Hubbell J H, Trehan P N, Singh N, Chand B, Mehta D, Garg M L, Garg R R, Singh S and Puri S 2004 *J. Phys. Chem. Ref. Data* **33** 621 (erratum)
Hubbell J H, Veigele W J, Briggs E A, Brown R T, Cromer D T and Howerton R J 1975 Atomic form factors, incoherent scattering functions, and photon scattering cross sections *J. Phys. Chem. Ref. Data* **4** 471–538
Hubbell J H, Veigele W J, Briggs E A, Brown R T, Cromer D T and Howerton R J 1977 *J. Phys. Chem. Ref. Data* **6** 615–6 (erratum)
ICRU 1984 *Stopping Powers for Electrons and Positrons, ICRU Report* 37 (Bethesda, MD: International Commission on Radiation Units and Measurements)
ICRU 2007 *Elastic Scattering of Electrons and Positrons, ICRU Report* 77 (Bethesda, MD: International Commission on Radiation Units and Measurements)
Inokuti M 1971 Inelastic collisions of fast charged particles with atoms and molecules—the Bethe theory revisited *Rev. Mod. Phys.* **43** 297–347
Inokuti M, Itikawa Y and Turner J E 1978 Addenda: inelastic collisions of fast charged particles with atoms and molecules—the Bethe theory revisited *Rev. Mod. Phys.* **50** 23–35

Inokuti M and Smith D Y 1982 Fermi density effect on the stopping power of metallic aluminum *Phys. Rev.* B **25** 61–6

James R W 1948 *The Optical Principles of the Diffraction of X-rays* (London: G Bell and Sons)

Jarp S and Mork K J 1973 Differential cross sections for pair production by photons on electrons *Phys. Rev.* D **8** 159–68

Jensen K O and Walker A B 1993 Monte Carlo simulation of the transport of fast electrons and positrons in solids *Surf. Sci.* **292** 83–97

Kawrakow I and Bielajew A F 1998 On the condensed history technique for electron transport *Nucl. Instrum. Methods* B **142** 253–80

Kawrakow I and Rogers D W O 2001 *The EGSnrc Code System: Monte Carlo Simulation of Electron and Photon Transport, Report* PIRS-701 (Ottawa: National Research Council of Canada)

Kim L, Pratt R H, Seltzer S M and Berger M J 1986 Ratio of positron to electron bremsstrahlung energy loss: an approximate scaling law *Phys. Rev.* A **33** 3002–9

Kim Y K, Santos J P and Parente F 2000 Extension of the binary-encounter-dipole model to relativistic incident electrons *Phys. Rev.* A **62** 052710

Kissel L, Quarles C A and Pratt R H 1983 Shape functions for atomic-field bremsstrahlung from electrons of kinetic energy 1–500 keV on selected neutral atoms $1 \leqslant Z \leqslant 92$ *At. Data Nucl. Data Tables* **28** 381–460

Kissel L, Zhou B, Roy S C, Sen Gupta S K and Pratt R H 1995 The validity of form-factor, modified-form-factor and anomalous-scattering-factor approximations in elastic-scattering calculations *Acta Cryst.* **A51** 271–88

Koch H W and Motz J W 1959 Bremsstrahlung cross-section formulas and related data *Rev. Mod. Phys.* **31** 920–55

Kolbenstvedt H 1967 Simple theory for K-ionization by relativistic electrons *J. Appl. Phys.* **38** 4785–7

Latter R 1955 Atomic energy levels for the Thomas–Fermi and Thomas–Fermi–Dirac potentials *Phys. Rev.* **99** 510–9

Liberman D, Cromer D T and Waber J T 1971 Relativistic self-consitent field program for atoms and ions *Comput. Phys. Commun.* **2** 107–13

Mayol R and Salvat F 1990 Cross sections for K-shell ionisation by electron impact *J. Phys. B: At. Mol. Opt. Phys.* **23** 2117–30

Møller C 1932 Zur Theorie des Durchgangs schneller Elektronen durch Materie *Ann. Phys.* **14** 531–85

Mork K J 1967 Pair production by photons on electrons *Phys. Rev.* **160** 1065–71

Mott N F and Massey H S W 1965 *The Theory of Atomic Collisions* 3rd edn (London: Oxford University Press)

Motz J W, Olsen H A and Koch H W 1969 Pair production by photons *Rev. Mod. Phys.* **41** 581–639

Nelson W R, Hirayama H and Rogers D W O 1985 *The EGS4 Code System, Report* SLAC-265 (Stanford, CA: Stanford Linear Accelerator Center)

Nikjoo H, Uehara S, Emfietzoglou D and Cucinotta F A 2006 Track-structure codes in radiation research *Radiat. Meas.* **41** 1052–74

Øverbø I, Mork K J and Olsen H A 1973 Pair production by photons: exact calculation for unscreened atomic field *Phys. Rev.* A **8** 668–85

Perkins S T, Cullen D E, Chen M H, Hubbell J H, Rathkopf J and Scofield J 1991 *Tables and Graphs of Atomic Subshell and Relaxation Data Derived from the LLNL Evaluated Atomic Data Library (EADL), Z = 1–100*, vol 30 *Report* UCRL-50400 (Livermore, CA: Lawrence Livermore National Laboratory)

Pratt R H 2006 Tseng's calculations of low energy pair production *Radiat. Phys. Chem.* **75** 624–30

Pratt R H, Levee R D, Pexton R L and Aron W 1964 K-shell photoelectric cross sections from 200 keV to 2 MeV *Phys. Rev.* **134** A898–915

Pratt R H, Ron A and Tseng H K 1973 Atomic photoelectric effect above 10 keV *Rev. Mod. Phys.* **45** 273–325

Pratt R H, Ron A and Tseng H K 1973 *Rev. Mod. Phys.* **45** 663–4 (erratum)

Pratt R H, Tseng H K, Lee C M and Kissel L 1977 Bremsstrahlung energy spectra from electrons of kinetic energy $1\,\text{keV} \leqslant T_1 \leqslant 2000\,\text{keV}$ incident on neutral atoms $2 \leqslant Z \leqslant 92$ *At. Data Nucl. Data Tables* **20** 175–209

Pratt R H, Tseng H K, Lee C M and Kissel L 1981 *At. Data Nucl. Data Tables* **26** 477–81 (erratum)

Rehr J J and Albers R C 2000 Theoretical approaches to x-ray absorption fine structure *Rev. Mod. Phys.* **72** 621–54

Ribberfors R 1975 Relationship of the relativistic Compton cross section to the momentum distribution of bound electron states *Phys. Rev.* B **12** 2067–74

Ribberfors R and Berggren K-F 1982 Incoherent-x-ray-scattering functions and cross section $(\mathrm{d}\sigma/\mathrm{d}\Omega')_{\text{incoh}}$ by means of a pocket calculator *Phys. Rev.* A **26** 3325–33

Richter W A and Brown B A 2003 Nuclear charge densities with the Skyrme Hartree–Fock method *Phys. Rev.* C **67** 034317

Rose M E 1961 *Relativistic Electron Theory* (New York: Wiley)

Sakurai J J 1967 *Advanced Quantum Mechanics* (New York: Addison-Wesley)

Salvat F 2003 Optical-model potential for electron and positron elastic scattering by atoms *Phys. Rev.* A **68** 012708

Salvat F, Fernández-Varea J M and Sempau J 2006 PENELOPE-*2006: A Code System for Monte Carlo Simulation of Electron and Photon Transport* (Issy-les-Moulineaux, France: OECD/NEA Data Bank) http://www.nea.fr/lists/penelope.html

Salvat F, Fernández-Varea J M and Williamson W Jr 1995 Accurate numerical solution of the radial Schrödinger and Dirac wave equations *Comput. Phys. Commun.* **90** 151–68

Salvat F, Jablonski A and Powell C J 2005 ELSEPA—Dirac partial-wave calculation of elastic scattering of electrons and positrons by atoms, positive ions and molecules *Comput. Phys. Commun.* **165** 157–90

Sauter F 1931 Über den atomaren Photoeffekt in der K-Schale nach der relativistischen Wellenmechanik Diracs *Ann. Phys.* **11** 454–88

Schiff L I 1951 Energy-angle distribution of thin target bremsstrahlung *Phys. Rev.* **83** 252–3

Scofield J H 1978 K- and L-shell ionization of atoms by relativistic electrons *Phys. Rev.* A **18** 963–70

Scofield J H 1989 Angular and polarization correlations in photoionization and radiative recombination *Phys. Rev.* A **40** 3054–60

Segui S, Dingfelder M, Fernández-Varea J M and Salvat F 2002 The structure of the Bethe ridge. Relativistic Born and impulse approximations *J. Phys. B: At. Mol. Opt. Phys.* **35** 33–53

Segui S, Dingfelder M and Salvat F 2003 Distorted-wave calculation of cross sections for inner-shell ionization by electron and positron impact *Phys. Rev.* A **67** 062710

Seltzer S M 1988 in *Monte Carlo Transport of Electrons and Photons* ed T Jenkins *et al* (New York: Plenum) pp 103–10

Seltzer S M and Berger M J 1985 Bremsstrahlung spectra from electron interactions with screened atomic nuclei and orbital electrons *Nucl. Instrum. Methods* B **12** 95–134

Seltzer S M and Berger M J 1986 Bremsstrahlung energy spectra from electrons with kinetic energy 1 keV–10 GeV incident on screened nuclei and orbital electrons of neutral atoms with Z = 1–100 *At. Data Nucl. Data Tables* **35** 345–418

Shimizu R and Ding Z-J 1992 Monte Carlo modelling of electron–solid interactions *Rep. Prog. Phys.* **55** 487–531

Slater J C 1951 A simplification of the Hartree–Fock method *Phys. Rev.* **81** 385–90

Sternheimer R M 1952 The density effect for the ionization loss in various materials *Phys. Rev.* **88** 851–9

Sternheimer R M, Seltzer S M and Berger M J 1982 Density effect for the ionization loss of charged particles in various substances *Phys. Rev.* B **26** 6067–76
Sternheimer R M, Seltzer S M and Berger M J 1983 *Phys. Rev.* B **27** 6971 (erratum)
Tessier F and Kawrakow I 2008 Calculation of the electron–electron bremsstrahlung cross-section in the field of atomic electrons *Nucl. Instrum. Methods* B **266** 625–34
Tsai Y S 1974 Pair production and bremsstrahlung of charged leptons *Rev. Mod. Phys.* **46** 815–51
Tseng H K and Pratt R H 1971a Exact screened calculations of atomic-field pair production and low-energy screening *Phys. Rev.* A **4** 1835–43
Tseng H K and Pratt R H 1971b Exact screened calculations of atomic-field bremsstrahlung *Phys. Rev.* A **3** 100–15
Tseng H K and Pratt R H 1973 Comments on screening and shell-ratio effects in single-quantum pair annihilation *Phys. Rev.* A **7** 1423–6
Walker D W 1971 Relativistic effects in low energy electron scattering from atoms *Adv. Phys.* **20** 257–323
Wheeler J A and Lamb W E 1939 Influence of atomic electrons on radiation and pair production *Phys. Rev.* **55** 858–62
Wheeler J A and Lamb W E 1956 *Phys. Rev.* **101** 1836 (erratum)
X-5 Monte Carlo Team 2003 *MCNP—A General Monte Carlo N-Particle Transport Code, Version 5, Report No* LA-UR-03-1987 (Los Alamos, NM: Los Alamos National Laboratory)

View publication stats